AN ABSTRACT OF THE THESIS OF

Congcong Hu for the degree of Doctor of Philosophy in Materials Science presented on November 20, 2019.

Title: Machine Learning Applied to Non-periodic Event Detection – A Special Case in Structural Health Monitoring.

Abstract approved:

_____

Roberto Albertani

Structural Health Monitoring (SHM) is known as the process of implementation of damage detection and characterization strategy. The method is widely used in modern critical equipment to minimize the risk of failures. While a significant effort has been devoted by researchers for the detection of faults in situations including periodic dynamic loads, there are no generally recognized methods for the identification of a non-periodic event, especially those with low signal-to-noise ratio (SNR). In this research, the case of an impact on wind turbines blades, as a typical non-periodic event during normal turbine operations, was studied using the newly developed advanced SHM method with implementation of support vector machine, a machine learning algorithm, explicitly, developed for the case with low SNR. Field tests were performed to collect data from vibration sensors installed on blades with artificial impacts obtained by launching tennis balls toward the blades' trajectory. Pre-processing showed that nearly half of the recorded impact events were successfully identified by visual inspection or by performing short-time Fourier transform. The present research

covers visually undetectable impact events, masked under background noise due to low SNR. Numerically simulated impacts on blades at various levels of SNR were used to perform an analysis of various training methods for the machine learning impact detection algorithm. Performance of the trained prediction model was evaluated using filed experimental data. Results on the feasibility and the efficiency of new proposed support vector machine algorithm including its optimization and accuracy were reported.

Machine Learning Applied to Non-periodic Event Detection – A Special Case in Structural Health Monitoring

by

Congcong Hu

A THESIS

submitted to

Oregon State University

in partial fulfillment of
the requirements for the
degree of

Doctor of Philosophy

Presented November 20, 2019

Commencement June 2020

Doctor of Philosophy thesis of Congcong Hu presented on November 20, 2019

APPROVED:

Major Professor, representing Materials Science

Director of the Materials Science Program

Dean of the Graduate School

I understand that my thesis will become part of the permanent collection of Oregon State University libraries. My signature below authorizes release of my thesis to any reader upon request.

Congcong Hu, Author

ACKNOWLEDGEMENTS

I could not have completed this research without assistance from many people. The people listed below are those who contributed directly to this thesis, but many other people have helped me along the way. I thank them all for making my experience at Oregon State University great.

I would like to express many thanks to my main advisor, Dr. Roberto Albertani, for his guidance and support throughout my research. I would not make it without his encouragement and patience. Also, many other faculty members at Materials Science department have helped me along the way. Thanks to Dr. Brian Bay, Dr. Bill Warnes and Dr. David Cann for getting me onto the right track of graduate program. Thanks also to my thesis committee members, including Dr. Solomon Yim, Dr. Matthew Johnston, Dr. Brian Bay and Dr. Wei Kong, for their support and valuable suggestions. Special recognition is necessary for my coworkers, especially Kyle Clocker, Will Maurer, Cole Anderson and Alexander Muschler. They have never failed to offer a helping hand, share their knowledge, and suggest good ideas. I cannot thank them enough. Finally, thanks to my family. I could not get this far without their support.

Sincerely,

Congcong Hu

CONTRIBUTION OF AUTHORS

Dr. Roberto Albertani helped in many aspects of this work including technical support, making suggestions on simulation methods and data analysis. He also helped with reviewing and revising the manuscript and this thesis. Dr. Robert M. Suryan helped with reviewing and revising the first manuscript.

TABLE OF CONTENTS

TABLE OF CONTENTS (Continued)

TABLE OF CONTENTS (Continued)

LIST OF FIGURES

LIST OF FIGURES (Continued)

LIST OF TABLES

1 INTRODUCTION

Most of engineering structures and machinery, such as bridges, wind turbines and transportation systems, are regulated by the application of codes, supported by various analyses, to ensure safety operations throughout the desired equipment's working life. Structures may be characterized by extreme design, include imperfection in materials, or experience extreme loading conditions. In all those cases machinery or structures may be functional while suffering from damages, or a shorter operating life. It is therefore highly desirable to monitor its working condition including possible changes in materials such as aging, fatigue, corrosion, delamination or other factors that can weaken the designed structure. Thus, it's of vital importance that critical structures are under continuous monitoring and evaluation for damage detection and characterization on a regular basis to minimize the risk of failures.

1.1 Structural Health Monitoring

The process of implementation of damage detection and characterization strategy is known as Structural Health Monitoring (SHM). Traditional SHM methods include visual inspection, non-destructive testing (NDT) techniques such as eddy current, ultrasound, and other wave-propagation-based methods [1]. As an example, the recent accident of a Southwest airlines flight potentially caused by an invisible crack in a fan blade in one of its two turbofan engines reminds the public of the risk of imperfection in materials or components, even for sophisticated items such as the nickel-based alloy engine blades. The engine blades are fully inspected for quality control purposes both during and after the production line [2]. In production process, X-ray dye is the most

commonly used technique for inspection of metal forging flaws. Ultrasound test is usually carried out as well to ensure that there are no weak spots in the part. As a results of the Southwest airlines accident, a new FAA directive specified that for certain CFM International S.A. (CFM) CFM56-7B turbofan engines ultrasonic inspection needed to be performed on fan blades due to the in-flight fan blade failure [3]. By these methods, specifically trained personnel are able to detect most of the hidden defects. However, the accuracy and effectiveness of such inspections depend heavily on accessibility of structural locations and the expertise of individuals performing the inspections. Furthermore, many of the current NDT methods cannot provide continuous information on the conditions of the system while in operation. The most widely applied engineering solution for continuous machine or structure monitoring is represented by SHM, which includes the implementation of automatic data collection and post processing or real-time evaluation. The ultimate goal of SHM is to predict the conditions of the system in the future by observing the present and using information from the past.

Traditional SHM involves three key steps [2, 4]:

(1) The observation of a system over time using sample of periodic dynamic response measurements from an array of sensors.

(2) The extraction of damage-sensitive features from these measurements. Time-frequency analysis, which introduces various techniques that can identify local and transient characteristic features in the vibration signal, is most commonly used in feature extraction in SHM [2, 5, 6].

(3) Statistical analysis of these features to determine the current health state of the system. The implemented algorithms analyze statistical distributions of identified features allowing to distinguish between undamaged and damaged structures as well as enabling the prediction of potential future damage.

1.2 Machine Learning

Machine learning is usually defined as giving computers or software applications the ability to learn without being explicitly programmed. Supervised and unsupervised learning are two categories in the field of machine learning. In the case of supervised learning, a known data set of input and output is referred to as the training examples. An algorithm to learn the mapping function from the input to the output is part of the progress. Once the mapping function is developed, new output can be predicted by new input data. For unsupervised learning, there are no output values and the main task of learning is to gain some understanding of the process which generated the data. The main difference between supervised and unsupervised learning is that the algorithms for supervised learning need training data from the testing system, while those for unsupervised learning do not. Support Vector Machine (SVM) is under the category of supervised learning. It is one of the most widely used frameworks for general classification and regression problems such as text categorization, image classification, biosequence analysis, and others. Features of an event or example can be extracted and then represented as a point in SVM space. Using a non-probabilistic binary linear classifier, SVM divides the space into two categories in which each point is assigned to one category or the other. For instance, in the field of SHM, signals collected from

a healthy structure (i.e. events) can be assigned to either healthy or faulty category. As a new technique for data classification developed since early 2000s, SVM fits the scope of feature extraction and statistical analysis in SHM, and hence has attracted special attention.

1.3 A SPECIAL CASE IN SHM

Vibration-based monitoring techniques are well developed and widely adopted by modern wind turbines for the purpose of sutural health monitoring [24]. Vibration sensors such as piezoelectric accelerometers are commonly installed on wind turbines for the analysis of dynamic structural response during operations [25, 26]. A lot of effort has been made by researchers for the detection of periodic faulty in rotating parts such as blades, bearings and gearbox under dynamic loads, by identifying its characteristic features in the vibration signal. However, there is no existing methods/techniques for automated non-periodic event detection, which is defined as a special case in SHM. This work proposes a robust method for non-periodic event detection under the general framework of SHM. Instead of traditional statistical analysis involved in SHM, a predictive model is constructed by implementation of SVM trained by extracted local and transient features that are sensitive to the non-periodic event from the vibration signals.

One of the major ecological concerns of the deployment of wind farms is the potential threat to bird species due to collisions with wind turbines [8-10]. Studies of bird and bat mortality rates for collisions with utility-scale wind turbines have reported an

estimate of up to 40 deaths per turbine per year on certain sites [11-13]. It is imperative that the development of offshore wind facilities will include efforts to minimize negative impact on bird and bat species, especially those that are listed as endangered or threatened. Common methodologies for bird/bat collision assessments and mortality rate monitoring include carcass survey and long-term visual observation [14-17]. However, due to surveyor efficacy and carcass removal by scavengers, the count could be inaccurate, and the true magnitude of the problem could be underestimated [17]. One approach for effective and low-cost automatic detection of bird/bat collision with wind turbines is to perform structural monitoring by the implementation of vibrational or acoustic sensing devices. The conceptual design of a multi-sensor system that provides both temporal and spatial coverage capacities for auto-detection of bird collision events was carried out at Oregon State University (OSU) based on prior bird collision monitoring systems [27-28]. Field testing was performed on utility-scale wind turbines. Artificial collision events were created by launching tennis balls into moving blades using compressed-air cannon. The preliminary results showed that it is feasible to detect an impact using common vibration sensors by visual inspection [29]. However, vibration signals that contain low-intensity impacts embedded in relatively high background noise are often characterized by low detection rate or low signal-to-noise ratio (SNR). In such case, neither visual identification nor conventional signal processing methods is feasible in identifying the impact event. Therefore, more advanced signal processing algorithms need to be developed for higher detection rate, especially for those impacts with relatively low SNR.

1.4 RESEARCH OBJECTIVE

By conducting this research, a robust method based on SVM is applied to vibration signal processing. In perspective of general SHM framework, the method is developed with the specific and original objective of the detection of non-periodical events in the presence to a low signal-to-noise ratio. The feasibility and efficiency of the proposed method applied to wind turbine blade impact detection are evaluated by simulation experiments. Finally, the proposed method is validated using filed experimental data.

1.5 References

1. Carden E.P., Fanning P. Vibration Based Condition Monitoring: A Review. *Structural Health Monitoring*. 2004; 3(4).
2. Isermann, Rolf. *Fault-Diagnosis Systems: an Introduction from Fault Detection to Fault Tolerance*. Springer, 2011.
3. Federal Aviation Administration (FAA), DOT. *Airworthiness Directives; CFM International S.A. Turbofan Engines*. August, 2017.
4. Martinez-Luengo M., Kolios A., Wang L. Structural health monitoring of offshore wind turbines: A review through the Statistical Pattern Recognition Paradigm. *Renewable and Sustainable Energy Reviews*. 2016; 64 (91-105).
5. Kumar A., Kumar R. Time-frequency analysis and support vector machine in automatic detection of defect from vibration signal of centrifugal pump. *Measurement*. 2017; 108(119-133).
6. Farrar C. R., Worden K. An introduction to structural health monitoring. *Phil. Trans. R. Soc. A*. 2007; 365(303-315).
7. Schwartz M, Heimiller D, Haymes S, Musial W. *Assessment of Offshore Wind*

Energy Resources for the United States. NREL/TP-500-45889; 2010

8. Bailey H, Brookes KL, Thompson PM. Assessing environmental impacts of offshore wind farms: lessons learned and recommendations for the future. *Aquatic Biosystems*. 2014;10(8)
9. homsen K. *Offshore Wind: A Comprehensive Guide to Successful Offshore Wind Farm Installation*. London: Elsevier Science; 2014.ISBN 9780124095946
10. Flowers J, Albertani R, Harrison T, Polagye B, Suryan RM. Design and Initial Component Tests of an Integrated Avian and Bat Collision Detection System for Offshore Wind Turbines. In: Marine Energy Technology Symposium; April 15–18, 2014; Seattle
11. Sovacool BK. Contextualizing avian mortality: A preliminary appraisal of bird and bat fatalities from wind, fossil-fuel, and nuclear electricity. *Energy Policy*. 2009;37(6):2241–2248
12. Marques AT, Batalha H, Rodrigues S, Costa H, Pereira MJR, Fonseca C, Mascarenhas M, Bernardino J. Understanding bird collisions at wind farms: An updated review on the causes and possible mitigation strategies. *Biological Conservation*. 2014;179:40–52
13. Al Zohbi G., Hendrick P., Bouillard Ph. Evaluation of the impact of wind farms on birds: the case study of Lebanon. *Renewable Energy*. 2015; 80(682-689).
14. Kunz T, Arnett EB, Cooper BM, Erickson WP, Larkin RP, Mabee T, Morrison ML, Strickland MD, Szewczak JM. Assessing Impacts of Wind-Energy Development on Nocturnally Active Birds and Bats: A Guidance Document. *Journal of Wildlife Management*. 2007;71(8):2449–2486

15. Korner-Nievergelt F., Brinkmann R., Niermann I., Behr O. Estimating bat and bird mortality occurring at wind energy turbines from covariates and carcass searches using mixture models. *PLOS ONE*. 2013; 8(7).
16. Parise J., Walker T. Industrial wind turbine post-construction bird and bat monitoring: A policy framework for Canada. *Journal of Environmental Management*. 2017; 201(252-259).
17. Smallwood KS. Long search intervals underestimate bird and bat fatalities caused by wind turbines. *Wildlife Society Bulletin*. 2017; 41(2): 224-230.
18. Sovacool B, Lindboe HH, Odgaard O. Is the Danish Wind Energy Model Replicable for Other Countries*? Electricity Journal*. 2008;21(2):27–38
19. lonczkier P, Simms IC. Radar monitoring of migrating pink-footed geese: behavioural responses to offshore wind farm development. *Journal of Applied Ecology*. 2012;49(5):1187–1194.10.
20. Brabant R, Vanermen N, Stienen EWM, Degraer S. Towards a cumulative collision risk assessment of local and migrating birds inNorth Sea offshore wind farms. *Hydrobiologia*. 2015;756:63–74.11.
21. Fijn RC, Krijgsveld KL, Poot MJM, Dirksen S. Bird movements at rotor heights measured continuously with vertical radar at a Dutch offshore wind farm. *Ibis*. 2015;157(3):558–566.12.
22. Towsey M, Wimmer J, Williamson I, Roe P. The use of acoustic indices to determine avian species richness in audio-recordings of the environment. *Ecological Informatics*. 2014;21:110–119.13.
23. Masden EA, Cook ASCP. Avian collision risk models for wind energy impact

assessments. *Environmental Impact Assessment Review*. 2016;56:43–49

24. Marquez FPG, Tobias AM, Perez JMP, Papaelias M. Condition monitoring of wind turbines: Techniques and methods. *Renewable Energy*. 2012;46:169–178.
25. bouhnik A, Albarbar A. Wind turbine blades condition assessment based on vibration measurements and the level of an empirically decomposed feature. *Energy Conversion and Management*. 2012;64:606–613.16.
26. Bassett K, Carriveau R, Ting DS. Vibration response of a 2.3 MW wind turbine to yaw motion and shut down events. *Wind Energy*.2011;14(8):939–952.17.
27. Wiggelinkhuizen EJ, Rademakers LWMM, Barhorst SAM, Boon HJ, Dirksen S, Schekkerman H. WT-bird: Bird collision recording for offshore wind farms. In: European Wind Energy Conference; Feb. 27–Mar. 2, 2006; Athens.18.
28. Desholm M, Fox AD, Beasley PDL, Kahlert J. Remote techniques for counting and estimating the number of bird wind turbine collisions at sea: a review. *Ibis*. 2006;148(s1):76–89
29. Hu C., Albertani R., Suryan RM. Wind turbine sensor array for monitoring avain and bat collisions. *Wind Energy*. 2018.

2 BACKGROUND THEORY

2.1 TIME-FREQUENCY ANALYSIS

All methods are based on the post processing analysis of signals recorded, from the interested machine or structure, in a time-based dimension. The goal is to perform such analysis in real time. Time-frequency analysis methods are widely used in the identification of local and transient characteristic features in vibration signals. One of the common techniques for performing time-frequency analysis is short-time Fourier transform (STFT). For the computation of STFT, a longer time-series signal is divided into shorter segments of equal length, and then, the Fourier transform is calculated separately on each shorter segment [1]. Due to the fixed width of the windowing function of STFT, there is always a trade between time resolution and frequency. In opposite to STFT, wavelet transform (WT) is computed by the frequency-dependent window. WT allows good time resolution for high frequencies, which is not possible in the case of STFT [1]. In this work, STFT and resulting spectrogram are performed for the evaluation of signal quality. Continuous wavelet transform (CWT) is carried out in the process of feature extraction in non-periodic event detection.

2.2 SUPPORT VECTOR MACHINE

As a supervised learning model, SVM adopts a discriminant function, also known as classifier, to classify if an event/example is positive or negative (i.e., 1 or -1). The fundamental of SVM is illustrated in Figure 2.1 using a linear classifier. In this case, each example can be represented by bold $\boldsymbol{x}$, which denotes a vector with component $\boldsymbol{x_i}$

(e.g., i=1, 2 in two-dimensional space, i=1, 2, 3 in three-dimensional space). A linear classifier is based on the discriminant function of the form [2]:

$$f(x) = w^T x + b \tag{1}$$

The vector w is known as the weight vector, which is a unit vector always perpendicular to the classifier. The term b is called the bias, which shifts the classifier away from the origin. When the discriminant function equals zero, the expression [2]

$$f(x) = w^T x + b = 0 \tag{2}$$

defines a hyperplane dividing the space into two regions (i.e. categories). It is a line in two dimensions or a plane in three dimensions. The side of an example (i.e. a point) is denoted by the sign of the discriminant function. In the illustration of two-dimensional space as shown in Figure 2.1, the hyperplane (the boldface straight line) divides all examples into two sides based on the sign of discriminant function: points marked by cross have positive sign, and those marked by circles are negative.

For a given hyperplane the closest points (circled points in Figure 2.1) to the hyperplane among positive and negative examples are denoted by x_+ and x_-. From simple geometric considerations the margin of a hyperplane with respect to a dataset (i.e. all events/examples) can be defined as [2]

$$m = \frac{1}{2} w^T (x_+ - x_-) \tag{3}$$

The maximum margin classifier is then defined as the hyperplane which has the maximum margin between positive and negative examples for linear separable dataset.

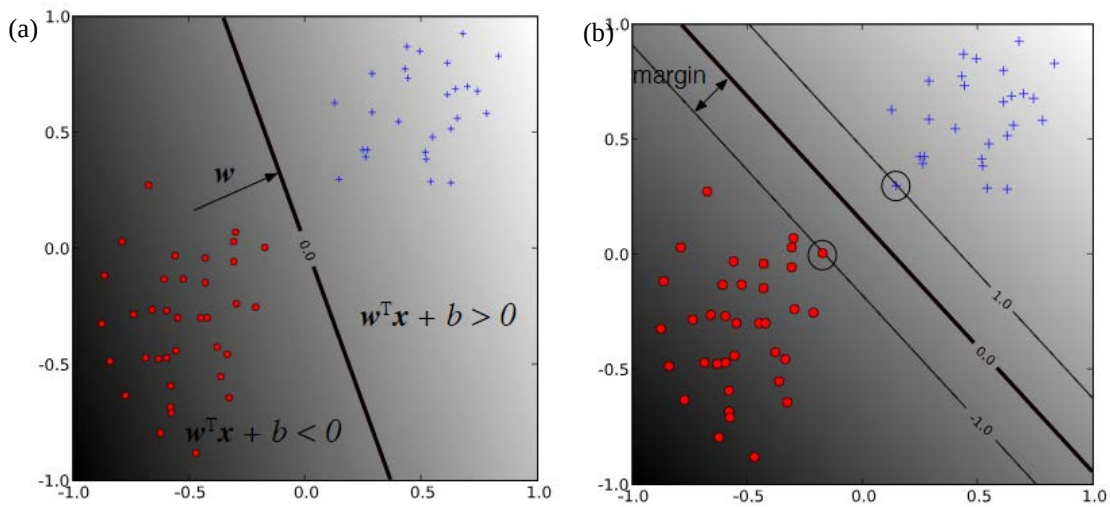

Figure 2.1: Illustration of linear classifier in SVM [2]. The two plots illustrate the concepts of linear classifier and margin selection in two-dimensional space case.

This technique can be applied to identify abnormal events in vibration data from dynamic structures on the extracted features, especially in the field of Structural Health Monitoring (SHM) [3, 4]. Training data are required for the implementation of the discriminant function. For instance, in the case of impacts on wind turbine blades, vibration sensors need to be installed on the blade for the collection of the structural responses to positive (impact) or negative (normal operation without impact) events. The methodology applied for the training process is illustrated in Figure 2.2. Figure 2.2(a) shows the time-series vibration signal collected by sensors deployed on a wind turbine blade. Multiple events were identified as independent training examples. A

positive (i.e. 1) or negative (i.e. -1) label was assigned to each example with or without an impact, as illustrated in Figure 2.2(b). A classifier is implemented by calculating the maximal margin between positive and negative events in an n-dimensional space, where n is the number of features extracted from raw signals of each example. In Figure 2.2(c), it was assumed to have only two features for each example, which formed a two-dimensional space. Finally, the calculated max-margin classifier allows the computer to automatically predict if a future event is with (positive) or without impact (negative). In real applications, vibration data are usually complex and noisy therefore they cannot be separated neatly by simple linear classifier as shown in Figure 2.2(c).

For the purpose of a desired linear separation, the data need to be transformed from low dimensional space into higher dimensional space. Therefore the kernel function, $K(x_i, x_j)$, is introduced to map examples in lower dimensions to higher dimensions [5]. The following four basic kernels are most common:

- linear: $K(\mathbf{x}_i, \mathbf{x}_j) = \mathbf{x}_i^T \mathbf{x}_j$,
- polynomial: $K(\mathbf{x}_i, \mathbf{x}_j) = (\gamma {\mathbf{x}_i}^T \mathbf{x}_j + r)^d,\ \gamma > 0$,
- radial basis function (RBF): $K(\mathbf{x}_i, \mathbf{x}_j) = \exp(-\gamma \|\mathbf{x}_i - \mathbf{x}_j\|^2),\ \gamma > 0$,
- sigmoid: $K(\mathbf{x}_i, \mathbf{x}_j) = \tanh(\gamma {\mathbf{x}_i}^T \mathbf{x}_j + r)$,

where γ, r and d are kernel parameters. The RBF kernel is generally preferred [2, 5, 6] and is used in this work.

With the data sets formed by training features provided by the time-frequency analysis, the predictive model is constructed based on SVM, and is used to classify if an impact event is contained in non-periodic signals.

2.3 References

1. Newland DE. *An Introduction to Random Vibrations, Spectral & Wavelet Analysis*. Courier Corporation, 2012.
2. Ben-Hur A., Weston J. *A User's Guide to Support Vector Machines*. 2010. http://pyml.sourceforge.net/doc/howto.pdf
3. Bornn L., Farrar CR., Park G., Farinholt K. Structural health monitoring with autoregressive support vector machines. *Journal of Vibration and Acoustics*. 2009; 131.
4. Regan T., Beale C., Inalpolat M. Wind turbine blade damage detection using supervised machine learning algorithms. *Journal of Vibration and Acoustics*. 2017; 139.
5. Hsu CW., Chang CC., Lin CJ. *A Practical Guide to Support Vector Classification*. 2003. https://www.csie.ntu.edu.tw/~cjlin/papers/guide/guide.pdf
6. Cristianini N., Shawe-Taylor J. *An Introduction to Support Vector Machines and Other Kernel-based Learning Methods*. Cambridge University Press, 2000.

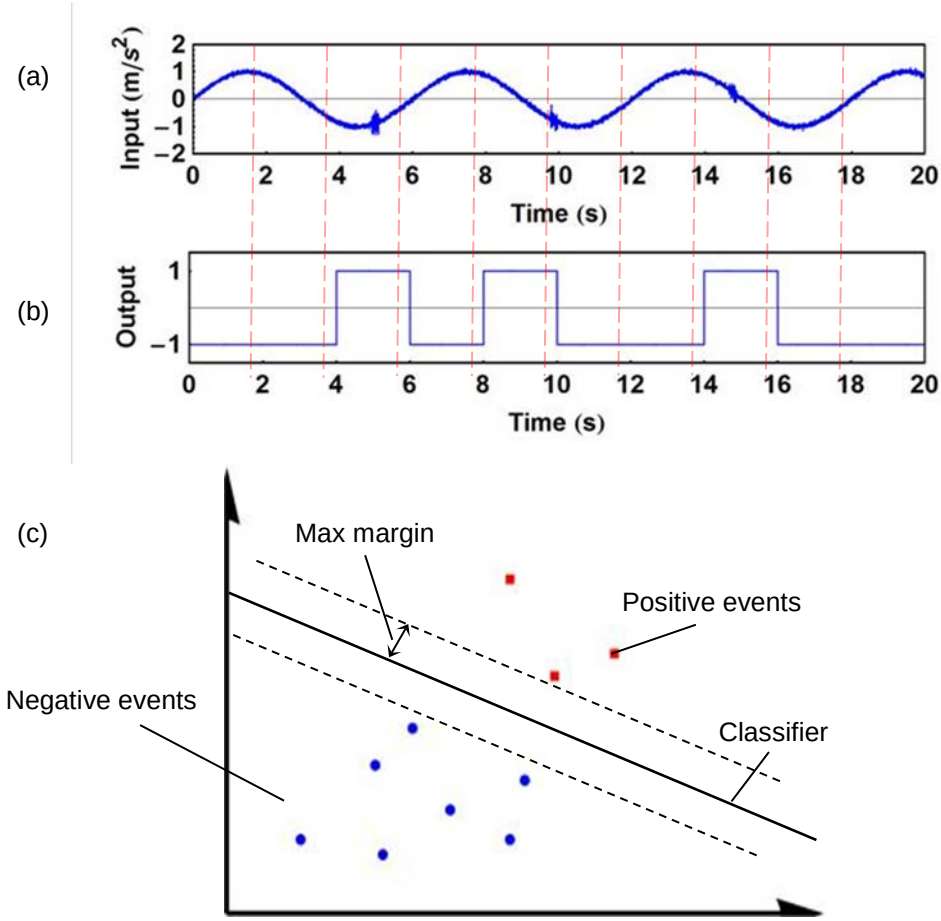

Figure 2.2: Example illustrating the training process of the Support Vector Machine with a maximal margin classifier. (a) Time series data of simulated signal for vibration sensor deployed on the wind turbine blade with three impacts. Ten events (every two seconds) were identified as independent inputs of training examples. (b) Plot shows labeling of the output for each training example. In this illustration, the seven events without an impact were labeled negative (-1) and the three with an impact were labeled positive (1). (c) Two-dimensional space formed by all ten examples. A classifier was implemented by calculating the maximal margin between positive and negative events.

3 MANUSCRIPT 1

Wind Turbine Sensor Array for Monitoring Avian and Bat Collisions

Congcong Hu[1]; Roberto Albertani[1]; Robert M. Suryan[2, 3].

Published in

Wind Energy

2018, Volume 21: 255-263.

[1]School of Mechanical, Industrial and Manufacturing Engineering, Oregon State University, Corvallis, Oregon, USA

[2]Department of Fisheries and Wildlife, Oregon State University, Hatfield Marine Science Center, Newport, Oregon, USA

[3]NOAA Fisheries, Alaska Fisheries Science Center, Auke Bay Laboratories, Ted Steven's Marine Research Institute, Juneau, Alaska, USA

3.1 ABSTRACT

Assessment of avian and bat collisions with wind turbines is necessary to ensure that the benefits of renewable wind power generation are not outweighed by mortality of protected species. An onboard, integrated multi-senor system capable of providing detection of turbine collision events, including taxonomic information, was developed. The conceptual design of a multi-sensor system including a vibration sensing node, an optics node, and an bioacoustic node with an event-driven trigger architecture was field-tested on utility-scale wind turbines. A pixel density computational model was built to estimate the spatial coverage and target resolution to the optimized configuration for camera placement. Field test results of the vibration node showed that nearly half of the recorded impact events were successfully identified by visual inspection and running short-time Fourier transform on recorded vibration signals. The remaining undetected impact events were masked under background noise due to low impact energy and high background noise of the operating turbine which result in subsequent low signal-to-noise ratio. Our results demonstrate the feasibility of triggering the system through single impact event sensed by vibration sensors.

3.2 INTRODUCTION

In recent years, wind energy generation is experiencing rapid worldwide development and is expected to play a significant role in the coming decades. In the United States, a total gross offshore wind energy potential of 4150 gigawatts (GW) was estimated by the National Renewable Energy Laboratory (NREL) [1]. However, the deployment of offshore wind farms brings environmental concerns such as interactions with marine life, increased noise, alterations to food resources, and disturbance to the seabed [2].

One of the major ecological concerns is the potential threat to marine bird species due to collisions with wind turbines [3, 4]. Studies of bird and bat mortality rates for collisions with utility-scale wind turbines have reported an estimate of up to 40 deaths per turbine per year on certain sites [5, 6]. It is imperative that the development of offshore wind facilities will include efforts to minimize negative impact on bird and bat species, especially those that are listed as endangered or threatened.

Common methodologies applied at land-based wind farms for bird/bat collision assessments and mortality rate monitoring are carcass survey and long-term visual observation [7], made generally at the scale of a single wind farm. Due to surveyor efficacy and carcass removal by scavengers, the count could be inaccurate, and the true magnitude of the problem could be underestimated. Most importantly, carcass surveys are expensive or infeasible at some sites, such as agricultural fields, dense shrub habitats, remote locations, and offshore. Common methodologies used to estimate potential interactions with offshore wind facilities are visual surveys (aerial and boat based), radar monitoring, and acoustic recordings that can inform collision risk models based on flux data [8-13]. Although these methodologies are powerful tools for the assessment of displacement effects of local birds and barrier effects of the wind farms on birds during migration, they are poorly suited for directly monitoring of collision events with wind turbines. Hence, effective and low-cost methods of collision event monitoring are required. Such approaches should include on-board systems with automatic collision detection, provide information for taxonomic identification, feature automatic monitoring, and ensure a long operational life with minimum maintenance.

One approach for automatic detection of bird/bat collision with wind turbines is abnormal event monitoring by the implementation of vibrational or acoustic sensing devices. Vibration-based monitoring techniques are well developed and widely adopted by modern wind turbines for rotating parts (e.g. blades, bearings, gearbox) [14]. Vibration sensors such as piezoelectric accelerometers are commonly installed on wind turbines for the analysis of dynamic structural response during operations [15, 16]. The WT-bird bird collision monitoring system [17] initially employed wired contact microphones (piezoelectric transducers sensitive to sound propagating through solid structures) on the blades before switching to wired accelerometers to improve durability and signal-to-noise ratios. Results have confirmed the feasibility of detection of collision events from structural vibration signals. Another approach, video surveillance (in either visual or infrared spectrum), also is widely employed by avian species monitoring systems. One notable infrared-based monitoring system is the Thermal Animal Detection System (TADS) [18], which was developed and applied to identify species through wing beat analysis and animal size. However, its collision detection function is not automatic, and a manual review of all collected imagery is required to assess the interactions of volant species with wind turbines.

Based on prior bird collision monitoring systems, this paper presents the conceptual design of a multi-sensor system that provides both temporal and spatial coverage capacities for auto-detection of bird collision events. Field testing was performed on utility-scale wind turbines. Testing details such as device positioning and sensor selection on the application of two main types of integrated vibration sensors (i.e.

accelerometer and contact microphone) are discussed. Artificial collision events were created by launching tennis balls into moving blades using compressed-air cannon. The objectives of this project are to test and evaluate signal qualities of common vibration sensors on non-stationary wind turbines to determine the feasibility of the designed multi-sensor system, and to serve as some basis to help develop advanced auto-detection systems for bird collision event monitoring in the future.

3.3 System description and testing

3.3.1 Multi-sensor system overview

The design of the on-board multi-sensor system under daylight operations mainly consists of four components: 1) the vibration sensor node (accelerometers and contact microphones) installed on the root of the blade, 2) the optical node (visual cameras) aiming at the rotor plane, 3) the bioacoustics node (acoustic microphones) mounted outside the nacelle, and 4) the data acquisition system and central controller inside the nacelle. The schematic diagram of the system is shown in Figure 3.1. The vibration sensors provide continuous vibration monitoring, while the optical and acoustic nodes acquire necessary information (i.e. visual images, impact sounds, and animal calls) for event confirmation and species recognition when an impact is detected. Since continuous data acquisition by the optical node at frame rates sufficient to capture fast-moving objects will produce a prohibitory volume of data to be archived, requiring massive post-processing, the event-driven trigger architecture has been developed to address this challenge. Each node continuously streams data into a ring buffer for temporary storage. When an event (e.g. collision) is registered by the vibration node, all buffers will store data in an operator-determined time window (e.g. equal temporal

period of temporal data on both sides of a triggered event), and eventually, all buffered data will be asynchronously stored on disk. This architecture minimizes the volume of data archived and enhances efficiency of data post-processing.

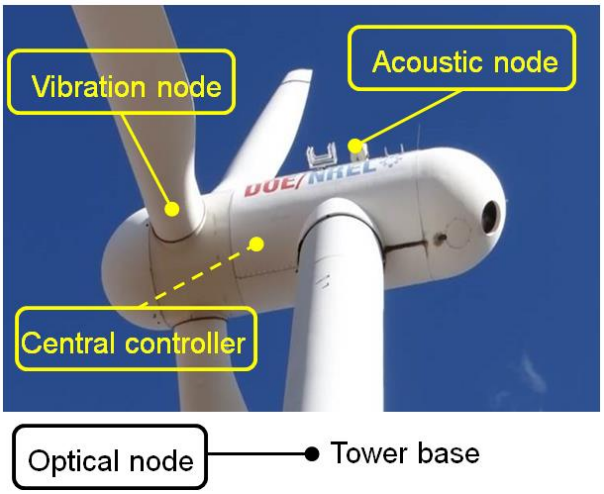

Figure 3.1: Schematic diagram of the auto-detect system with event-driven trigger architecture on NREL CART3 wind turbine.

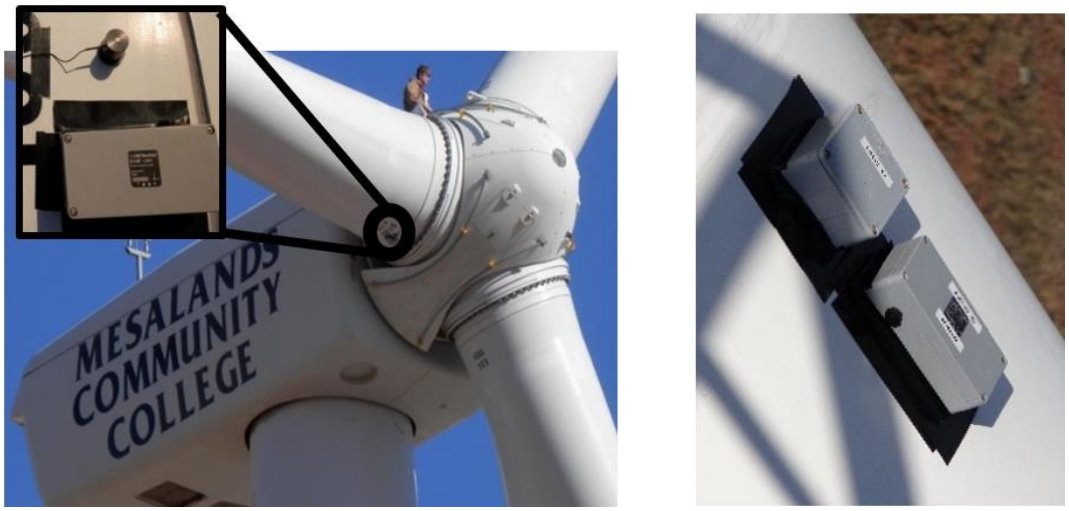

Figure 3.2: Sensor placement: vibration sensors mounted on the blade including (a) 1.5 MW GE wind turbine at NAWRTC (b) 600 kW CART3 wind turbine at NREL-NWTC.

3.3.2 Vibration node

The sensing of blade vibrations was tasked as the primary triggering source for image acquisition and impact confirmation. As such, particular attention was devoted to testing two different sensors for the same function with the objective to ultimately select the more practical sensor. The two sensors were 1) wireless three-axis accelerometers (LORD MicroStrain G-Link LXRS w/ 104-LXRS base station), and 2) wireless contact microphones (Sun-Mechatronics USK-40 w/ UZ-10 UHF receiver). Two per blade, they formed the vibration node, providing continuous structural vibration monitoring and collision event trigger in the event-driven architecture. The sensors with weatherproof housing were installed at the root of the blades, as shown in Figure 3.2, for easier accessible installation, easy maintenance, and negligible aerodynamic effects on the blades. The blade surface first was cleaned at the application location, and the housing box was applied to the surface with proper orientation (one axis parallel to the longitudinal axis of the blade) using 3M double bonding tape. The accelerometer signal was digitized prior to wireless transmission, while the contact microphone signal was transmitted as an analog signal, and was digitized by a NI USB-4431 DAQ (www.ni.com) at the receiver station. The receiver station containing paired wireless receivers was placed inside the nacelle next to the central controller. For timely processing of data for real-time collision monitoring, considering the processing ability of current hardware [16], sampling rates were chosen at 512 Hz for accelerometers and 1000 Hz for contact microphones.

3.3.3 Bioacoustics node

The bioacoustics node consisted of an acoustic microphone (G.R.A.S. general-purpose electronic piezoelectric microphone with frequency range of 10 to 20,000 Hz). The microphone was placed on top of the nacelle. In addition to species audio identification, it is valuable for environmental assessment that might lead to missed or false impact triggers (e.g. rain, lightning, etc.). Since no avian vocalizations were recorded due to the short timeframe of the testing, only acoustic recordings of turbine operation associated with an impact trigger used to trigger the system were collected, thus providing a proof of concept for an integrated bioacoustics node to be used as potential extra source of trigger.

3.3.4 Optical node

The implementation of optical cameras always involves the tradeoff between target resolution and field of view (FOV). In general, wider field of view would also result in lower target resolution. A target pixel density simulation model was developed to find the proper camera deployment location. With known camera specifications (i.e. effective focal length, sensor size, and image resolution), position (i.e. distance from camera to the rotor plane) and orientation, each pixel on the image can be projected (mapped) onto the rotor plane using trigonometric functions, as illustrated in Figure 3.3. For a given physical dimension on the rotor plane, the target resolution can be estimated as the sum of pixel pitches for all correlated pixels. Three options of optical node configurations are 1) on the nacelle, with a field of view that intersects the rotor plane, 2) on the turbine tower, near its base, in an upward-facing configuration, and 3) on an adjacent tower, viewing the entire rotor plane. During the field testing, option 2)

was tested with a visual camera (Currera-R RL50C-OC) deployed near the tower base with an upper angle of view targeting the blade rotor plane, due to the short testing timeframe.

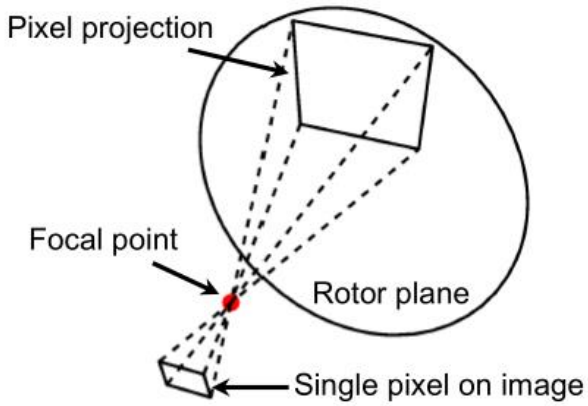

Figure 3.3: Illustration of pixel mapping.

3.3.5 System field tests

The required sub component functions and overall system functionality, reliability, and accuracy had to be validated in field tests with operating wind turbines and simulated bird impacts on the blades. Two locations for tests were selected for availability of wind turbines not involved in commercial energy conversion and for the excellent technical and logistic support on site. Partial system early tests were performed at the North American Wind Research and Training Center (NAWRTC) at the Mesalands Community College in Tucumcari, NM. The Center operates a General Electric GE 1.5 MW wind turbine. Later tests on the fully integrated system were performed at the National Renewable Energy Laboratory (NREL) National Wind Technology Center (NWTC) in Boulder, CO. The turbine used at the NWTC was the 600 kW CART3 (three blades).

In both cases, bird impacts were simulated by launching tennis balls using a custom compressed-air launcher, as illustrated in Figure 3.4. The cannon was barreled to the size of a regular tennis ball, and it was possible to launch one or two simultaneously. Three avian species (two offshore, one onshore) of regulatory concern include the marbled murrelet (*Brachyramphus marmoratus*), the short-tailed albatross (*Phoebastria albatrus*) and golden eagle (*Aquila chrysaetos*). They reflect a wide variety in body length and weight of 24 cm and 202 g for the murrelet, 70 cm and 3600 g for golden eagle, to 91 cm and 4680 g for the albatross. Specific bat species that were investigated include the hoary and silver-haired bats. They have body length of 11-15 cm and weight of 10-30 g. All species can fly at speeds up to 45 km/hour or more. When considering the impact kinetics, it is more likely that a bird/bat would be hit by

Figure 3.4: Air cannon is used to launch tennis balls to mimic bird impacts at NREL-NWTC.

the leading edge of a blade than the animal running into the rapidly moving face of the blade (up to 250 km/hr or more). Additionally, the tennis balls were launched from ground and flying in a parabolic trajectory before hit by the blade. Therefore, the impact kinetics is more a function of the object mass and the blade speed. Tennis ball mass was 57 g without water, and 140 g when filled with water, which is comparable to small birds or large bats. In addition, tennis balls were easy to launch and made no damage to the blade. Launch direction in reference to the rotor was downwind in the case of NAWRTC and upwind in the case of NREL-NWTC. Regulations at NREL prevented launching of balls from downwind toward the rotor, which at the NAWRTC allowed two passes to be made through the rotor, for medium and high wind, effectively doubling the probabilities of a blade strike.

Due to varying wind conditions, low impact rate, and short timeframe of field testing, a limited number of collision events was created and recorded. During field testing, the ring buffer duration was set for 10 s before and after impact of the tennis ball. All recordings were manually triggered to ensure that data are collected for later examination and post-processing. Field notes of visually observed impact events including time, position of impact, blade status, and weather conditions were taken and matched with output data acquired from each sensor node. Typical accelerometer and contact microphone data post-processing included 1) First stage with visual inspection of time histories for quality control purposes and for event detection, and 2) Second-stage processing including numerical signal analysis. In summary, a total of 23 dynamic impact (i.e. tennis balls hitting moving blades) events were successfully

obtained at NAWRTC, and six were obtained at NWTC under wind turbine normal operating condition (i.e. rotor at designed speed, generator engaged). The higher impact rate at NAWRTC was primarily caused by more favorable wind conditions. Likewise, four additional dynamic impact events were recorded at NWTC under turbine idle operation (i.e. blade free spinning, generator not engaged) due to low wind occurrence. The signal-to-noise ratio (SNR) was defined as follows:

$$SNR = 20\ long_{10} \frac{A_{impact}}{A_{noise}} \tag{1}$$

where A is the root mean square (RMS) amplitude, and was calculated and evaluated for all impacts.

3.4 Results and discussion

3.4.1 Signal quality of vibration node

Figure 3.5 shows a sample of the six time histories vibration data (two sensors per blade, three blades) collected at NAWRTC, which resulted from a single impact of a tennis ball on one blade. Signals from accelerometers are in the left column, with sensors labeled N543, N648, and N649, respectively. Signals from the three contact microphones are in the right column, with the sensors labeled A, B, and C. Although the ball was struck by one blade only, it is evident from the figure that two accelerometers and all three contact microphones had picked up the impact, demonstrating the generally higher sensitivity to impact detection of contact microphones. In our specific case, however, the wireless transmission protocol for the accelerometers was decisively more reliable than the contact microphones, resulting in an unpredictable and relevant loss of data for the latter system. Therefore, the choice

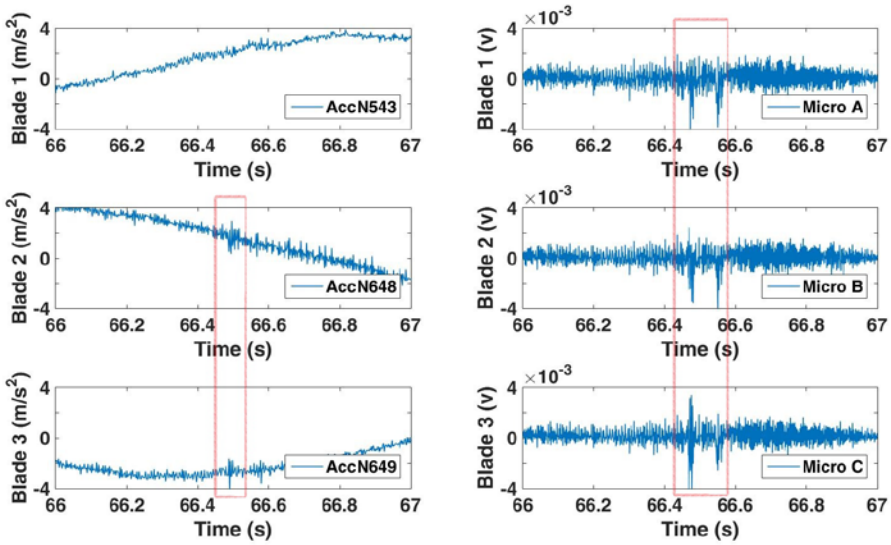

Figure 3.5: Sample time history plots showing vibration data collected by all six sensors (two sensors per blade, three blades) from a single impact event on one blade at NAWRTC for (a) accelerometers and (b) contact microphones. The impact can be identified through visual inspection on two accelerometers and three contact microphones.

of the accelerometers was the primary source of vibration data for post-processing and statistical analysis in the present work. In addition, the contact microphone exhibited consistently noisy signals, resulting in random false positive impact information. The wireless protocol of the accelerometers included a signal storage capability at the sensor level and a feature for automatic transmission repetition of data packets in the event of a lost connection.

3.4.2 Configuration of optical node

Using the target resolution simulation, the spatial coverage, which is defined as the percentage ratio between the camera surveillance area and the area of the blade rotor plane, as well as the target pixel resolution, was estimated using the turbine at the

NREL-NWTC as reference (rotor diameter of 40 m and nacelle length of 9 m). As an illustration, the camera was positioned at the rear end of the nacelle looking forward toward the rotor at an angle of 55 degrees upward from the horizontal plane. For an image resolution of 640x480 pixels and a focal length of 12 mm, Figure 3.6 shows a contour plot of pixel density for a target with dimensions of 240x240 mm on the rotor plane, assuming the target was struck by the blade. In this configuration, the camera provided a spatial coverage of 6.5% and minimum target resolution of more than 100 pixels. Three different camera positions, at the end of the nacelle, at the tower base, and on an adjacent tower at a distance of 200 m from the turbine, were evaluated using the same simulation model. Results, which are summarized in Table 1, illustrate spatial coverage and target resolution for a standard 240x240 mm object. As expected, the relation is inverse between camera coverage and image pixel resolution. The configuration on an adjacent tower provides more than 90% coverage at the expense of target resolution to a mere 20 pixels. The camera placed at the tower base offers up to 50% of coverage with a medium pixel density of 50. The negative characteristic of the above positions is the inability of the camera to follow the yawing of the nacelle, an impractical solution.

Table 3.1: Computational results of spatial coverage and target resolution for different camera configurations.

Camera location	Spatial coverage	Minimum target resolution (a 240x240 mm target)
On the nacelle	approximately 7%	more than 100 pixels
Near the tower base	approximately 50%	more than 50 pixels
On adjacent tower	approximately 90%	more than 20 pixels

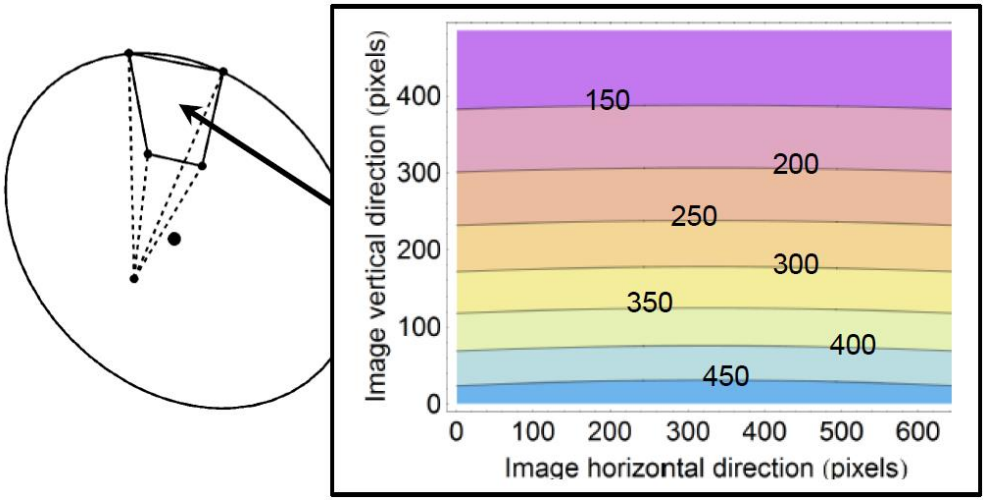

Figure 3.6: Contour plot of target resolution for single camera deployed on the nacelle.

3.4.3 Impact-driven architecture

Validation of the blade sensor-triggering capabilities was critical for system characterization. Simulations of blade collision events using tennis balls were conducted along different sections of the rotating blades during field testing. An example of a blade striking a tennis ball is also illustrated in Figure 3.7, showing the signal from the accelerometer mounted on the blade. The three time-histories represented from top to bottom are 1) NREL CART3 during normal operations producing energy, 2) NAWRTC GE during normal operations producing energy, and 3) NREL CART3 during idle with generator disengaged. Table 2 lists the results of average SNR and the corresponding coefficient of variation (CV) for each testing case. In all three plots in Figure 3.7, the noise in the signals correspond to the vibrations on the root of the blade, measured by the accelerometer. The spikes of impact were slightly ahead of the triggering events due to the reaction time of the recorder. As expected,

idle operations, shown in the bottom plot in Figure 3.7, are characterized by a lower background vibration noise which results the highest SNR due to the disengagement of the generator and low-power operation of the gearbox. In addition, Figure 3.7 and Table 2 reveal the generally lower background vibrations on the GE turbine with respect to the NREL CART3; this condition of higher SNR would improve the efficiency of data post-processing. The problem of automatically detecting a blade impact in the presence of noise at various, but predictable, frequencies could be solved by applying time-frequency analysis techniques, a common procedure in analyzing vibrations from rotating machines.

Table 3.2: Overview of signal-to-noise ratio for all impacts.

Cases	Number of impacts	Average SNR (dB)	CV (%)
CART3 600 kW normal operation	6	5.45	35.74
CART3 600 kW idle operation	4	14.59	37.01
GE 1.5 MW normal operation	23	7.03	33.05

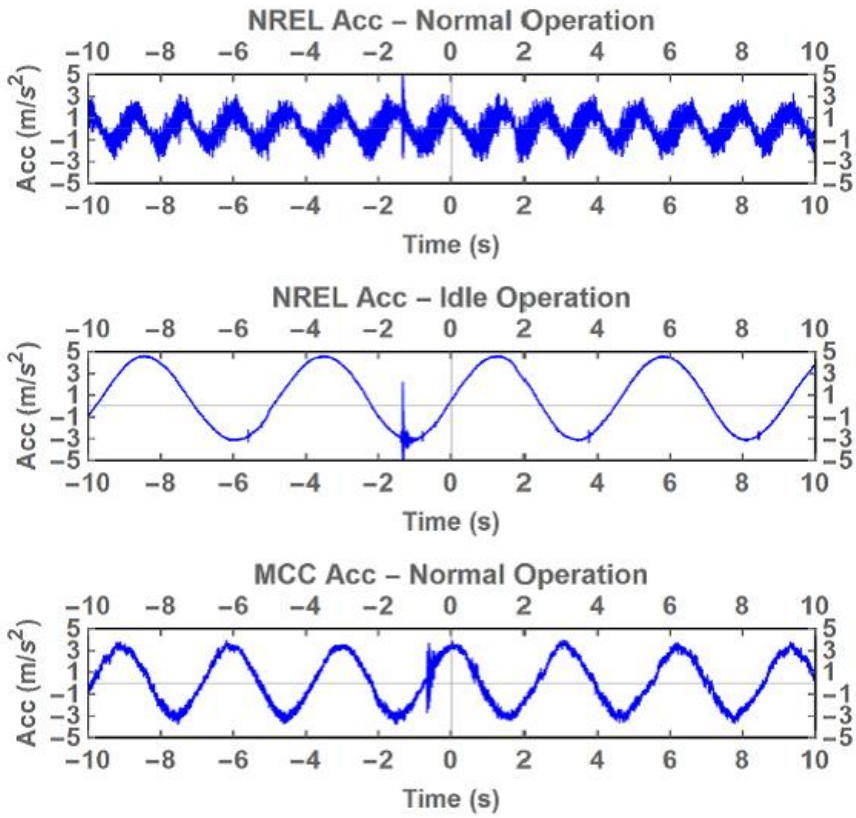

Figure 3.7: Accelerometer data from the CART3 600 kW turbine during normal operation and idle operation, and the GE 1.5 MW turbine during normal operation from top to bottom. Impacts were measured and can be seen on the plots at -1.33, -1.30 and -0.6 seconds, respectively.

The short-time Fourier transform (STFT) was applied to the accelerometer signals in second-stage data post-processing. The primary result of this method, a spectrogram, is illustrated in Figure 3.8. The spectrogram provides a visual representation of the frequency spectrum in the time window selected for post-processing. The technique was chosen for the potential application to detect impacts in real time. The example given in Figure 3.8 is the spectrogram obtained from the signal of the accelerometer installed on a blade of the NREL CART3 turbine during idle operation with the blade

hitting a tennis ball. The time history of the same event is illustrated on the left of Figure 3.8; it shows the acquired signals from the accelerometer with time on the vertical axis. The spectrogram exhibits a spike in the frequency domain at the time of the blade hitting the tennis ball, thus unequivocally identifying the strike. Frequency levels at different times represent typical turbine background vibrations due to blade aerodynamics, structural vibrations, bearings, gearbox, and various mechanical sources.

General results from 29 field tests with blade strikes showed the positive detection and confirmation of 14 events. The most probable cause of partial impact detection was the low-energy aspect of several events, with the result of a significantly low sensor signal-

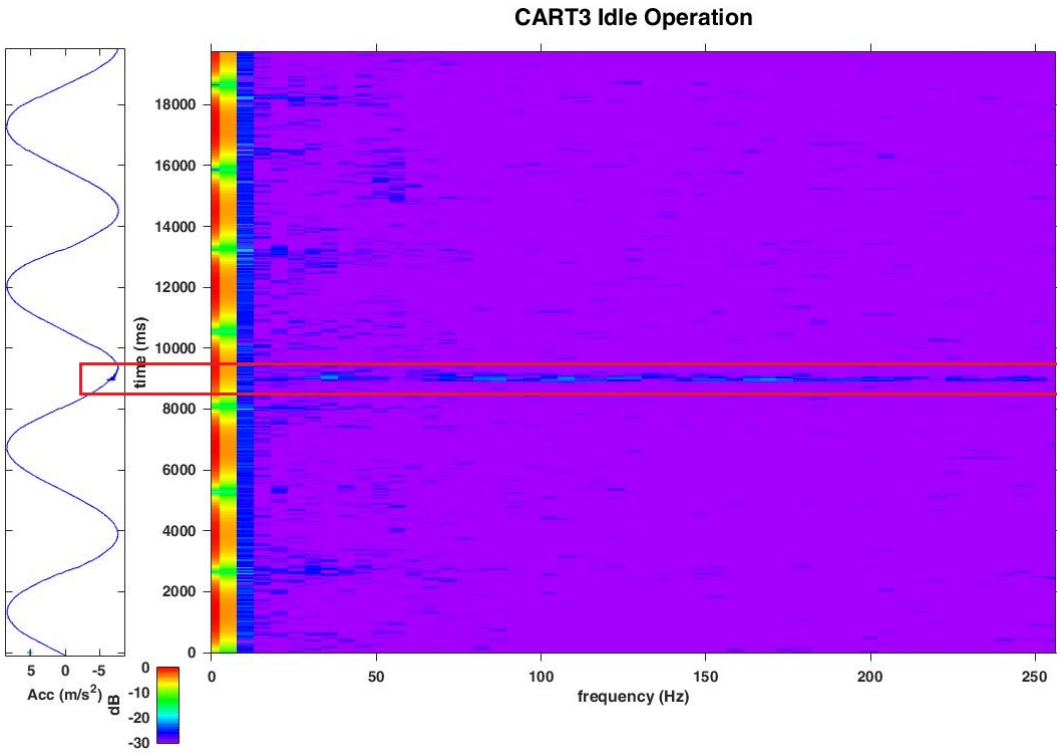

Figure 3.8: Illustration of acquired vibration data post-processing using STFT. The plot on the left shows the time history signal of the accelerometer installed on a blade of the CART3 turbine during idle operation. An impact was identified by its corresponding spectrogram, which exhibits a spike in the frequency domain.

to-noise ratio that cannot be detected with the current post-processing technique. Most of the detected strikes occurred at the leading edge of the blade and in a radial position between half blade and blade tip, thus at relatively high kinetic energy. Impacts during turbine idle operations are particularly favorable for detection due to the extremely low background noise measured by the sensors. A result of great interest was the capability of detecting a strike of a blade to a tennis ball by any of the sensors installed on the three blades, an indication that not necessarily all blades of a rotor need to be provided with sensors to detect impacts.

3.5 Conclusions

This study demonstrates through experimentation the feasibility of an impact detection system based on vibration sensors that are integrated into a multi-sensor array to detect and identify causes of blade impacts on wind turbines. Our study also highlights the necessity to validate any impact detection system by operating field tests on full-scale wind turbines in real operating conditions and by simulating bird impact on the blades. Results from this study elucidate several key characteristics and critical features for efficient automatic impact detection on wind turbine blades. The system can be adapted easily to any structure exposed to impact events. Cameras for impact confirmation and animal species recognition are critical, however, camera installation on the nacelle or any other fixed structure on or around the wind turbine has little practical value for the significantly small field of view with the minimum pixel density required for species recognition. Automatic triggering of the cameras using vibration sensors on the blades is an efficient technique, providing the sensors have a reliable wireless data

transmission, a high signal-to-noise ratio and, most important, an efficient and fast post-processing technique to discern the spike caused by the impact from the normal vibration background. Using a combination of visual impact detection by inspecting vibration signal time histories and running short-time Fourier transform, 14 out of 29 registered artificial impacts were detected, which corresponds to a 48.3% success rate. Considering a more efficient automatic detection event from vibration sensors, it is strongly believed that the success rate can be significantly increased. It is important to note that several impacts were successfully detected by sensors installed on blades other than the blade subjected to the impact. This is an indication that only one or two blades, out of three, could be instrumented with vibration sensors without decreasing the detection success rate significantly. However, it is required to have all three blades in the vision system field of view for event confirmation and animal species recognition. It was evident from the field tests that contact microphones have greater potential than accelerometers in terms of sensitivity and ease of signal processing. However, the low quality of wireless transmission of the available commercial contact microphones has hampered their use, and results from accelerometers were used primarily for impact detection. Bioacoustic microphones embedded in the system, providing they can record a signal relatively clean from background noise, can have a significant value in terms of event confirmation, can enhance species recognition in the presence of animal calls, and provide information on environmental variables affecting sensors such as rain, lightning, etc. Micro wireless visual sensors mounted directly on the blades have been tested briefly, with great success in terms of blade impact area coverage, species recognition, and potential for event detection.

3.6 Future work

With the general aims of improving automatic real-time impact detection, increasing video imaging coverage, and decreasing system energy requirements, the following improvements are suggested:

- Blade vibration sensors should have on-board data processing capabilities and transmit a packet of data only after the impact is detected;
- Sensor fusion should be applied to improve detection success rate;
- Sensor wireless transmission should rely on more efficient and standard wireless protocols;
- An efficient and fast event detection method should be applied, possibly with real-time signal filtering to decrease background noise and improve the detection success rate;
- Micro wireless visual sensors should be mounted directly on the blades to greatly increase critical impact area coverage;
- More tests should be carried out with the specific objective to establish the minimum number of vibration sensors on blades required for camera triggering;
- Micro infrared camera mounted on blades should be tested for night vision;
- Solar energy or rotational motion energy harvesting for sensor battery charging should be tested for increased autonomous and low-maintenance operations.

3.7 Acknowledgments

The authors wish to acknowledge the financial support of the U.S. Department of Energy under DE-EE0005363. The authors are grateful to the staff of the North

American Wind Research and Training Center at Mesalands Community College for contributing to the success of the systems first field test. The authors would also like to express gratitude to the staff and scientists at NREL for their willingness to share information with the team and for use of the Controls Advanced Research Turbines at the National Wind Technology Center for system testing and demonstration. Finally, we greatly appreciate the review and expert contributions of our science and industry advisory panel.

3.8 References

1. Schwartz M, Heimiller D, Haymes S, Musial W. *Assessment of Offshore Wind Energy Resources for the United States*. NREL/TP-500-45889; 2010.
2. Bailey H, Brookes KL, Thompson PM. Assessing environmental impacts of offshore wind farms: lessons learned and recommendations for the future. *Aquatic Biosystems*. 2014;10(8).
3. Thomsen K. *Offshore Wind: A Comprehensive Guide to Successful Offshore Wind Farm Installation*. London: Elsevier Science; 2014. ISBN 9780124095946.
4. Flowers J, Albertani R, Harrison T, Polagye B, Suryan RM. Design and Initial Component Tests of an Integrated Avian and Bat Collision Detection System for Offshore Wind Turbines. In: Marine Energy Technology Symposium; April 15–18, 2014; Seattle.
5. Sovacool BK. Contextualizing avian mortality: A preliminary appraisal of bird and bat fatalities from wind, fossil-fuel, and nuclear electricity. *Energy Policy*. 2009;37(6):2241–2248.

6. Marques AT, Batalha H, Rodrigues S, Costa H, Pereira MJR, Fonseca C, Mascarenhas M, Bernardino J. Understanding bird collisions at wind farms: An updated review on the causes and possible mitigation strategies. *Biological Conservation*. 2014;179:40–52.
7. Kunz T, Arnett EB, Cooper BM, Erickson WP, Larkin RP, Mabee T, Morrison ML, Strickland MD, Szewczak JM. Assessing Impacts of Wind-Energy Development on Nocturnally Active Birds and Bats: A Guidance Document. *Journal of Wildlife Management*. 2007;71(8):2449–2486.
8. Sovacool B, Lindboe HH, Odgaard O. Is the Danish Wind Energy Model Replicable for Other Countries?. *Electricity Journal*. 2008;21(2):27–38.
9. Plonczkier P, Simms IC. Radar monitoring of migrating pink-footed geese: behavioural responses to offshore wind farm development. *Journal of Applied Ecology*. 2012;49(5):1187–1194.
10. Brabant R, Vanermen N, Stienen EWM, Degraer S. Towards a cumulative collision risk assessment of local and migrating birds in North Sea offshore wind farms. *Hydrobiologia*. 2015;756:63–74.
11. Fijn RC, Krijgsveld KL, Poot MJM, Dirksen S. Bird movements at rotor heights measured continuously with vertical radar at a Dutch offshore wind farm. *Ibis*. 2015;157(3):558–566.
12. Towsey M, Wimmer J, Williamson I, Roe P. The use of acoustic indices to determine avian species richness in audio-recordings of the environment. *Ecological Informatics*. 2014;21:110–119.

13. Masden EA, Cook ASCP. Avian collision risk models for wind energy impact assessments. *Environmental Impact Assessment Review*. 2016;56:43–49.

14. Marquez FPG, Tobias AM, Perez JMP, Papaelias M. Condition monitoring of wind turbines: Techniques and methods. *Renewable Energy*. 2012;46:169–178.

15. Abouhnik A, Albarbar A. Wind turbine blades condition assessment based on vibration measurements and the level of an empirically decomposed feature. *Energy Conversion and Management*. 2012;64:606–613.

16. Bassett K, Carriveau R, Ting DS. Vibration response of a 2.3 MW wind turbine to yaw motion and shut down events. *Wind Energy*. 2011;14(8):939–952.

17. Wiggelinkhuizen EJ, Rademakers LWMM, Barhorst SAM, Boon HJ, Dirksen S, Schekkerman H. WT-bird: Bird collision recording for offshore wind farms. In: European Wind Energy Conference; Feb. 27–Mar. 2, 2006; Athens.

18. Desholm M, Fox AD, Beasley PDL, Kahlert J. Remote techniques for counting and estimating the number of bird wind turbine collisions at sea: a review. *Ibis*. 2006;148(s1):76–89.

4 MANUSCRIPT 2

Machine learning applied to wind turbine blades impact detection

Congcong Hu[1]; Roberto Albertani[1].

Published in

Wind Engineering

Online, 2019

[1]School of Mechanical, Industrial and Manufacturing Engineering, Oregon State University, Corvallis, Oregon, USA

4.1 ABSTRACT

The significant development of wind power generation worldwide brings, together with environmental benefits, wildlife concerns for volant species vulnerability to interactions with wind energy facilities. For surveying such events, an automatic system for continuous monitoring of blade collisions is critical. An onboard multi-senor system capable of providing real-time collision detection using integrated vibration sensors is developed and successfully tested. However, to detect low signal-to-noise ratio impact can be challenging hence an advanced impact detection method has been developed and presented in this paper. A robust automated detection algorithm based on support vector machine is proposed. After a preliminary signal pre-processing, geometric features specifically selected for their sensitivity to impact signals are extracted from raw vibration signal and energy distribution graph. The predictive model is formulated by training conventional support vector machine using extracted features for impact identification. Finally, the performance of the predictive model is evaluated by accuracy, precision and recall. Results indicate a linear regression relationship between signal-to-noise ratio and model overall performance. The proposed method is much reliable on higher signal-to-noise ratio (SNR$\geqslant$6), but it shows to be ineffective at lower signal-to-noise ratio (SNR<2).

4.2 Introduction

As an important component of renewable energy, wind energy generation has been growing at a fast pace in recent years due to its low cost and high availability [1-3]. Although the environmental impact associated with the usage of fossil fuel can be reduced by the clean alternative energy source, the deployment of an increased number

of wind facilities with larger scale turbines generates wildlife concerns for volant species such as birds and bats [4, 5]. Common causes of death for wildlife interacting with wind turbines include direct collision with turbines [6-9] and the risk of barotrauma especially for bats [10]. Among all the causes, direct collision with wind turbines is the most visible and well-documented impact as results of wind energy development [11].

Common methodologies applied at land-based wind farms for bird/bat fatality assessments are carcass surveys and long-term visual observation [6-8, 12], made generally at the scale of a single wind farm. Studies of bird and bat mortality rates from collisions with utility-scale wind turbines [13, 14] have reported an estimate of up to 40 deaths per turbine per year on certain sites. However, due to surveyor efficacy and carcass removal by scavengers, the count could be inaccurate, and the true magnitude of the problem could be underestimated [9]. Moreover, carcass survey and visual observation are characterized by high human operator's labor time, and are infeasible at certain sites, such as agricultural fields, dense shrub habitats, remote locations, and on water. Other methodologies [15-20] applied for estimation of potential interactions between volant species and wind facilities include aerial and boat-based visual surveys, radar monitoring, and acoustic recordings, which can be applied to collision risk models based on flux data. However, they are not suited for deterministic monitoring of collision events. Hence, effective and low-cost methods of continuous collision event monitoring with implementation of automatic data collection and evaluation have been sought by researchers in recent years [21].

Vibration-based monitoring techniques are widely adopted by modern wind turbines for rotating parts (e.g., brakes, bearings and gearboxes) [21]. Vibration sensors such as piezoelectric accelerometers are commonly installed on wind turbines for the analysis of dynamic structural response during operations [22, 23]. One notable approach for volant species collision detection is the conceptual design of a multi-sensor system developed by the authors [24]. By implementation of vibration sensors and surveillance cameras, the multi-sensor system can perform on-board collision detection, providing information for taxonomic identification, with minimal effort required to maintain long operational life. The preliminary results of field testing on utility-scale wind turbines proved the feasibility of collision detection using vibration sensors [24]. However, advanced signal processing methods need to be developed for a higher detection rate, especially for those impacts with relatively low signal-to-noise ratio (SNR), which typically involve bats and small birds such as the Marbled Murrelet.

Support vector machine (SVM) is one of the most widely applied frameworks for general classification problems such as condition monitoring and fault diagnosis [25]. Relevant features of an event can be extracted and then represented as a vector in SVM feature space. Non-probabilistic binary linear classifiers allow SVM to divide the feature space into different categories, enabling automatic prediction of a future event on its member category.

This paper presents a robust signal processing method based on SVM applied to automated impact detection. Firstly, geometric features associated with structure characteristics of impact signals are extracted from both raw vibration signals and energy distribution graph. Input vectors constructed by extracted features are then applied to train the SVM model, which is used for impact identification after training. The objectives of this study are to illustrate signal qualities of common vibration sensors on non-stationary wind turbine blades, and to evaluate the feasibility of proposed automated impact detection method using conventional support vector machine, especially for different levels of SNR.

The remainder of this paper is organized as follows. The theoretical background and proposed procedure are briefly described in section 2. Section 3 introduces the experimental data acquisition system, discusses field testing results, and illustrates the pre-processing methods on field-collected raw signals. To overcome the issue of rarity of bird collision events and limited number of artificial impacts, simulated studies are performed in Section 4. Finally, conclusions are drawn in Section 5.

4.3 Theoretical Background

4.3.1 Support Vector Machine

SVM is a supervised machine learning method introduced by [26], which is widely used in machine condition monitoring and fault diagnosis. The process of SVM for a binary classification problem is described as follows. Assume a sample dataset

$(x_i, y_i)_{i=1}^{N}$, where the notation x_i denotes thei^{th} vector in the dataset and y_i is the label associated with x_i. In binary classification, the positive and negative classes are labeled with $y_i = 1$ and $y_i = -1$, respectively. The discriminant function is of the form

$$f(x) = w^T x + b \tag{1}$$

where w is the weight vector, and b is the bias. Based on the discriminant function, a hyperplane defined by

$$f(x) = w^T x + b = 0 \tag{2}$$

divides the input space X into two classes: positive ($f(x) > 0$) and negative ($f(x) < 0$). To find the optimal hyperplane, the maximum margin criterion is applied, by which the optimal hyperplane is the hyperplane that gives the maximum distance between the decision boundary and the plane, as illustrated in Figure 4.1.

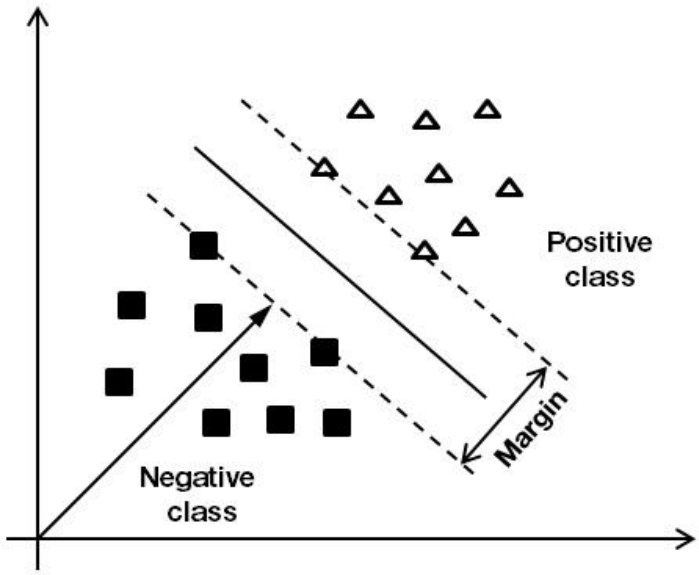

Figure 4.1. Illustration of linear classifier in two-dimensional space.

Considering noisy data that are not linearly separable, or to achieve a larger margin, misclassification is allowed by introducing slack variables $\xi_i > 0$ and error penalty $C > 0$. The problem can be expressed by the following constrained optimization problem:

$$\begin{aligned} &\text{Minimize} && \tfrac{1}{2}\|w\|^2 + C\sum_{i=1}^{n}\xi_i \\ &\text{Subject to} && y_i(w^T x_i + b) \geq 1 - \xi_i \end{aligned} \tag{3}$$

which is also known as soft-margin SVM [25]. Introducing Lagrange multipliers α_i, this optimization problem can be converted into the equivalent Lagrange dual formulation:

$$\begin{aligned} &\text{Minimize} \quad L(\alpha) = \sum_{i=1}^{N} \alpha_i - \frac{1}{2}\sum_{i=1}^{N} \alpha_i\, \alpha_j y_i y_j x_i^T x_j \\ &\text{Subject to} \quad \sum_{i=1}^{N} \alpha_i y_i = 0, 0 \leq \alpha_i \leq C. \end{aligned} \tag{4}$$

To define a nonlinear classifier, the input vector x_i is mapped from lower input space X into higher feature space F by mapping function $\Phi(x)$, which typically calculates using a dot product. However, the approach of explicitly mapping each input vector from the input space into the feature space results in quadratic complexity (i.e., quadratic increase in memory usage and quadratic increase in time required for computation). The kernel function $K(x_i, x_j) = \Phi^T(x_i) \cdot \Phi(x_j)$ is then introduced to solve the issue by skipping the step of explicitly mapping. The following four basic kernels are most commonly used:

- linear: $K(\mathbf{x}_i, \mathbf{x}_j) = \mathbf{x}_i^T \mathbf{x}_j$,
- polynomial: $K(\mathbf{x}_i, \mathbf{x}_j) = (\gamma {\mathbf{x}_i}^T \mathbf{x}_j + r)^d,\ \gamma > 0$,
- radial basis function (RBF): $K(\mathbf{x}_i, \mathbf{x}_j) = \exp(-\gamma \|\mathbf{x}_i - \mathbf{x}_j\|^2),\ \gamma > 0$,
- sigmoid: $K(\mathbf{x}_i, \mathbf{x}_j) = \tanh(\gamma {\mathbf{x}_i}^T \mathbf{x}_j + r)$,

The RBF kernel is generally preferred [25] and is applied in the present work.

Finally, the problem is converted into a “kernelized” dual quadratic optimization problem as follows:

$$\text{Minimize} \quad L(\alpha) = \sum_{i=1}^{N} \alpha_i - \frac{1}{2}\sum_{i=1}^{N} \alpha_i \, \alpha_j y_i K(x_i, x_j)$$
$$\text{Subject to} \quad \sum_{i=1}^{N} \alpha_i y_i = 0, 0 \leq \alpha_i \leq C. \tag{5}$$

This problem can be solved by the method of sequential minimal optimization [25]. The final discriminant function then has the expression of

$$f(x) = sign(\sum_{i=1}^{N} \alpha_i y_i K(x, x_i) + b). \tag{6}$$

4.3.2 Procedure for Impact Detection

In the present study, SVM has been proposed as the classification method; the procedure for the automatic impact detection using SVM is shown in Figure 4.2. The following steps are applied: 1) Raw vibration signal is collected by vibration sensors installed on the wind turbine blades; 2) Raw signal is pre-processed using continuous wavelet transform (CWT); 3) The time marginal integration (TMI) graph is obtained by calculating the energy distribution in CWT with respect to time (i.e., integrating CWT with respect to time for each scale); 4) Features are extracted from both raw signal and TMI graphs. The selected 18 features [27] are listed in Table 4.1; 6) The

SVM model is trained and tested by 10-fold cross-validation. Parameters γ and C are optimized by grid search in a grid of $2^{-10} - 2^{10}$.

Table 4.1. List of extracted features.

No.	Feature	Source	No.	Feature	Source
1	Kurtosis	Raw signal	10	Kurtosis	TMI signal
2	Skewness		11	Skewness	
3	Mean		12	Mean	
4	RMS		13	RMS	
5	Variance		14	Variance	
6	Peak		15	Peak	
7	Impulse factor		16	Impulse factor	
8	Shape factor		17	Shape factor	
9	Crest factor		18	Crest factor	

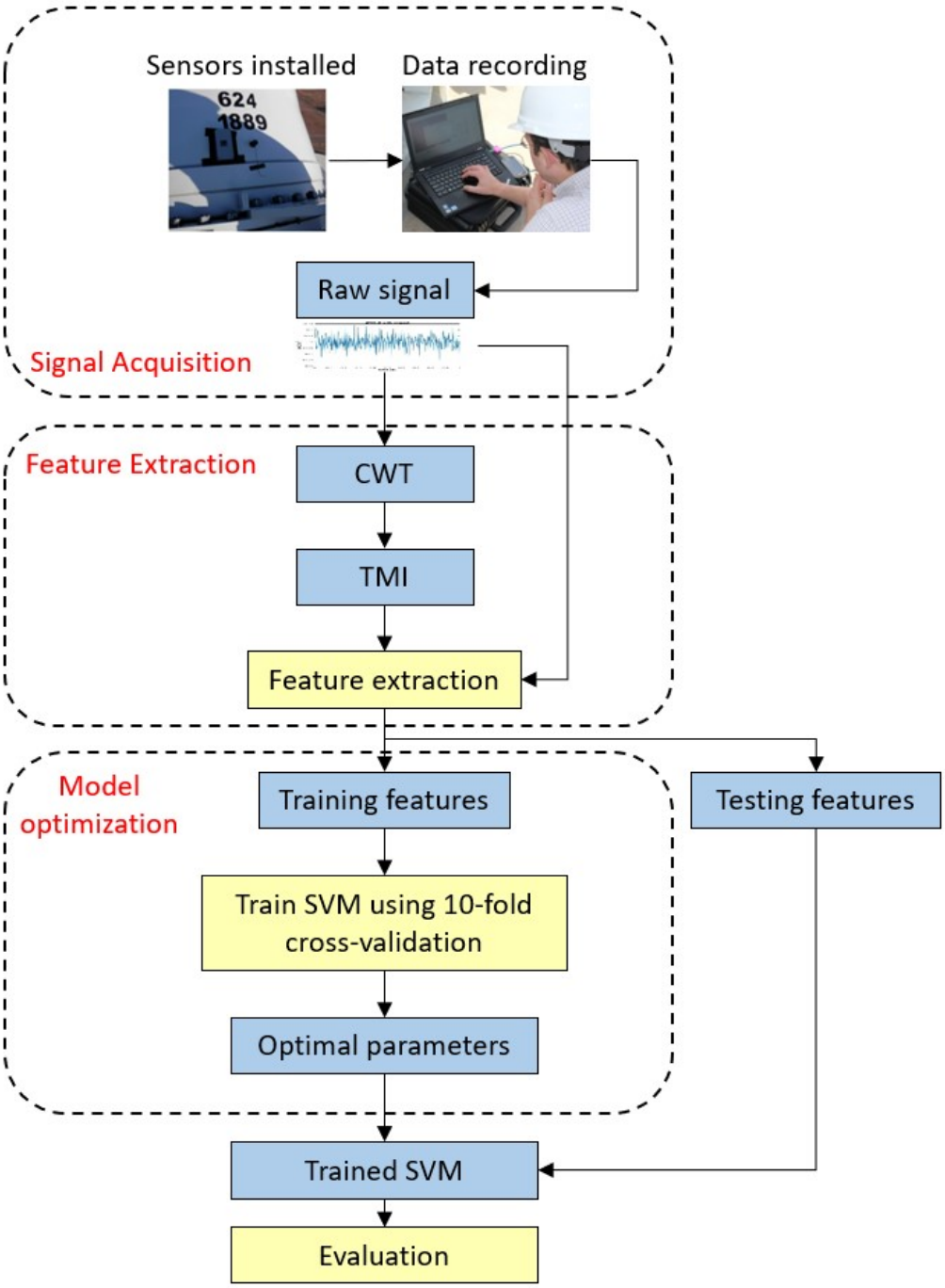

Figure 4.2. Flow chart of procedure for impact detection.

4.4 Experimental Evaluation

4.4.1 System Setup and Data Acquisition

The conceptual design of the on-board multi-sensor system under daylight operations was developed by the authors [24]. It primarily consists of: 1) Vibration sensor node (accelerometers) installed on the root of the blade, 2) Optical node (surveillance cameras) aiming at the rotor plane, 3) Bioacoustics node (acoustic microphones) mounted outside the nacelle, and 4) Data acquisition system and central controller inside the nacelle. The vibration sensors provide continuous vibration monitoring, while the optical and acoustic nodes acquire necessary information (i.e., visual images, impact sounds, and animal calls) for event confirmation and species recognition when an impact is detected. The event-driven trigger architecture was used to acquire data since continuous data acquisition by the optical node at frame rates sufficient to capture fast-moving objects will produce a prohibitory volume of data to be archived. Each node continuously streams data into a ring buffer for temporary storage. When an event (e.g., collision/impact) is registered by the vibration node, all buffers will store data in an operator-determined time window, which eventually will be asynchronously stored on disk. This architecture minimizes the volume of data archived and enhances efficiency of data post-processing.

Blade vibrations were selected as the primary triggering source of the system. Wireless three-axis accelerometers (LORD MicroStrain G-Link LXRS w/ 104-LXRS base station) were installed at the root of each blade with weatherproof housing, as shown

in Figure 4.3. The installation position was selected for easier accessible installation and maintenance, and negligible aerodynamic effects on the blades. For timely processing of data for real-time collision monitoring, considering the processing capabilities of the selected hardware, sampling rates were chosen at 512 Hz [22].

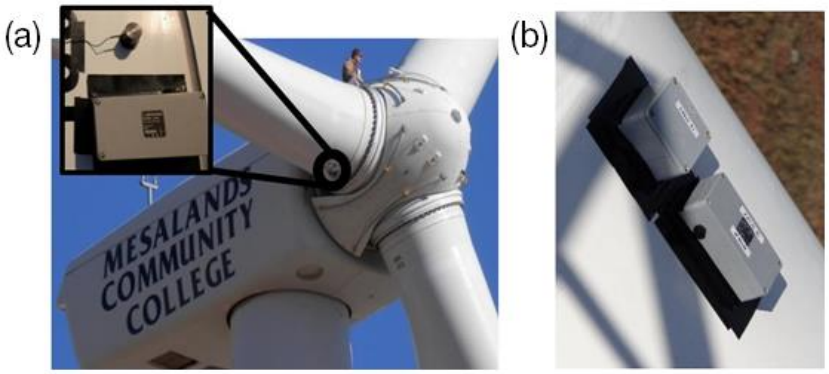

Figure 4.3. Experimental set-up of data acquisition system: (a) Installation of vibration node at the root of each blade; (b) housing of vibration node.

The overall system functionality, reliability, and accuracy were validated in field tests with operating wind turbines and simulated bird impacts on the blades. Two sites for field testing were selected for availability of wind turbines not involved in commercial energy conversion and for the excellent technical and logistic support on site. Partial system early tests were performed at the North American Wind Research and Training Center (NAWRTC) at the Mesalands Community College in Tucumcari, NM, on a General Electric (GE) 1.5 MW wind turbine. Later tests on the fully integrated system were performed at the National Renewable Energy Laboratory (NREL) National Wind

Technology Center (NWTC) in Boulder, CO. The turbine used at the NWTC was the 600 kW CART3 (three blades). In both cases, bird impacts were simulated by launching tennis balls using a custom compressed-air cannon, as illustrated in Figure 4.4. The cannon was barreled to the size of a regular tennis ball, whose mass was 57 g and 140 g when filled with water.

Figure 4.4. Simulation of bird impacts by launching tennis balls using an air cannon.

Development costs of the general system were covered by funds from the U.S. Department of Energy. Material costs, without considering improvement due to manufacturing efficiency and mass production, are estimated to be approximately 700 to 1,000 U.S. dollars per blade plus the cost for a computer laptop per turbine, after fixed costs for production tools are covered. Installation on a large size wind turbine requires approximately two persons for two to three days, including system set up and

basic functional tests. Real time blade-events monitoring is automatic including uploading of data and images to a storage system, cloud-based or similar, providing network or satellite link is available. Post events inspection of recorded images is currently based on visual interaction with human operators after the images are available after recording. Automatic computer-based inspection is possible as future development. Additionally, since blade damage was the most frequently reported damage occurrences among all other subsystems (i.e., gearbox, generator, transformer, foundation and other) [28], the proposed system may also serve for blade health monitoring. However, it will require better understanding on the turbine and blade structures [29] and further development of implemented diagnosis algorithms [30, 31].

4.4.2 Summary of Field Testing Results

Due to varying wind conditions, low impact rate, and short timeframe of field testing, a limited number of collision events was created and recorded. All recordings were manually triggered to ensure that the raw signal was collected for later examination and post-processing. Field notes of visually observed impact events including time, position of impact, blade status, and weather conditions were recorded and matched with output signals acquired from each sensor node. Preliminary examination, including visual inspection and signal processing using the short-time Fourier transform (STFT), was performed on-site on raw signals. In summary, 23 dynamic impact events (i.e., moving blade hitting tennis balls) were successfully obtained at NAWRTC, and six were obtained at NWTC under wind turbine normal operating condition (i.e., rotor at designed speed, generator engaged). The higher impact rate at NAWRTC was primarily

caused by more favorable wind conditions. Likewise, four additional dynamic impact events were recorded at NWTC under turbine idle operation (i.e., rotor free spinning, generator not engaged) due to low wind occurrence.

Raw signal examples of a blade striking a tennis ball are shown in Figure 4.5. The three time histories represented from top to bottom are (a) NREL CART3 during normal operations producing energy, (b) NREL CART3 during idle with generator disengaged, and (c) NAWRTC GE during normal operations producing energy. Table 4.2 lists the results of average SNR and the corresponding coefficient of variation (CV) for each testing case. The SNR was defined as follows:

$$SNR = 20log_{10}\frac{A_{impact}}{A_{noise}} \tag{7}$$

where A is the root mean square (RMS) amplitude and was calculated and evaluated for signal with impacts. In all three plots in Figure 4.5, the spikes of impact were slightly ahead of the triggering events due to the reaction time of the recorder. As expected, signals collected under idle operations are characterized with a lowest background vibration noise, resulting in a highest SNR due to the disengagement of the generator and low-power operation of the gearbox.

Table 4.2. Overview of SNR for all impacts.

Case	# of impacts	Avg. SNR (dB)	CV (%)
CART3 normal	6	5.45	35.74
CART3 idle	4	14.59	37.01
GE normal	23	7.03	33.05

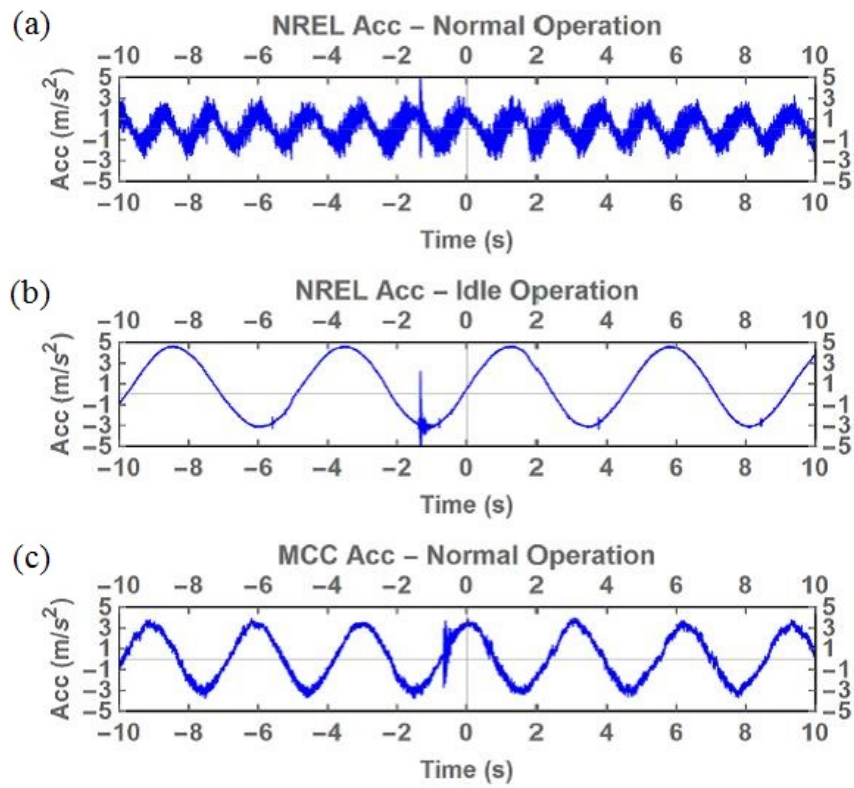

Figure 4.5. Illustration of vibration signals from accelerometers with different background noise: (a) NREL CART3 during normal operations producing energy; (b) NREL CART3 during idle operation with blade free spinning; (c) NAWRTC GE during normal operations producing energy.

Over the 29 blade-strike events under normal operation, only 14 can be confirmed by visual inspection, as illustrated in Figure 4.5, and by STFT. The most probable cause of this partial detection rate was the low-energy characteristic of several events due to the location of the impact close to the rotor shaft, which results in a significantly low SNR that cannot be identified using preliminary examination techniques. Most of the detected strikes occurred at the leading edge of the blade and in a radial position between half blade and blade tip, thus at relatively high kinetic energy. Impacts during turbine idle operations are particularly favorable for detection due to the extremely low background noise measured by the sensors.

4.4.3 Pre-processing of Raw Signals

For SVM data preparation, the raw signals were pre-processed. Figure 4.6 and Figure 4.7 illustrate the pre-processing steps using raw signals from both the GE and CART3 turbines under normal operation. The raw time histories of Figure 4.6 and Figure 4.7 are shown in Figure 4.5 bottom and top, respectively. A high-pass filter was applied to eliminate low-frequency components ($f \leq 5\ hz$) caused by blade rotation. Resultant time histories are shown in Figure 4.6 (a) and Figure 4.7 (a). This step was applied to eliminate the considerably large kinetic energy caused by blade rotation, which can easily dominate the energy distribution graph if presented. Figure 4.6 (b) and Figure 4.7 (b) show the scalograms as results of the continuous wavelet transform (CWT). CWT gives overall better time resolution for high-frequency components, which is essential for obtaining the energy distribution graph when integrating CWT with

respect to time. Figure 4.6 (c) and Figure 4.7 (c) are the energy distribution plots illustrated by TMI graphs. It is noted that impacts are better distinguishable in TMI graphs than in CWT plots. Features listed in Table 4.1 are then extracted from the raw signal and the TMI graph to obtain a training and testing dataset.

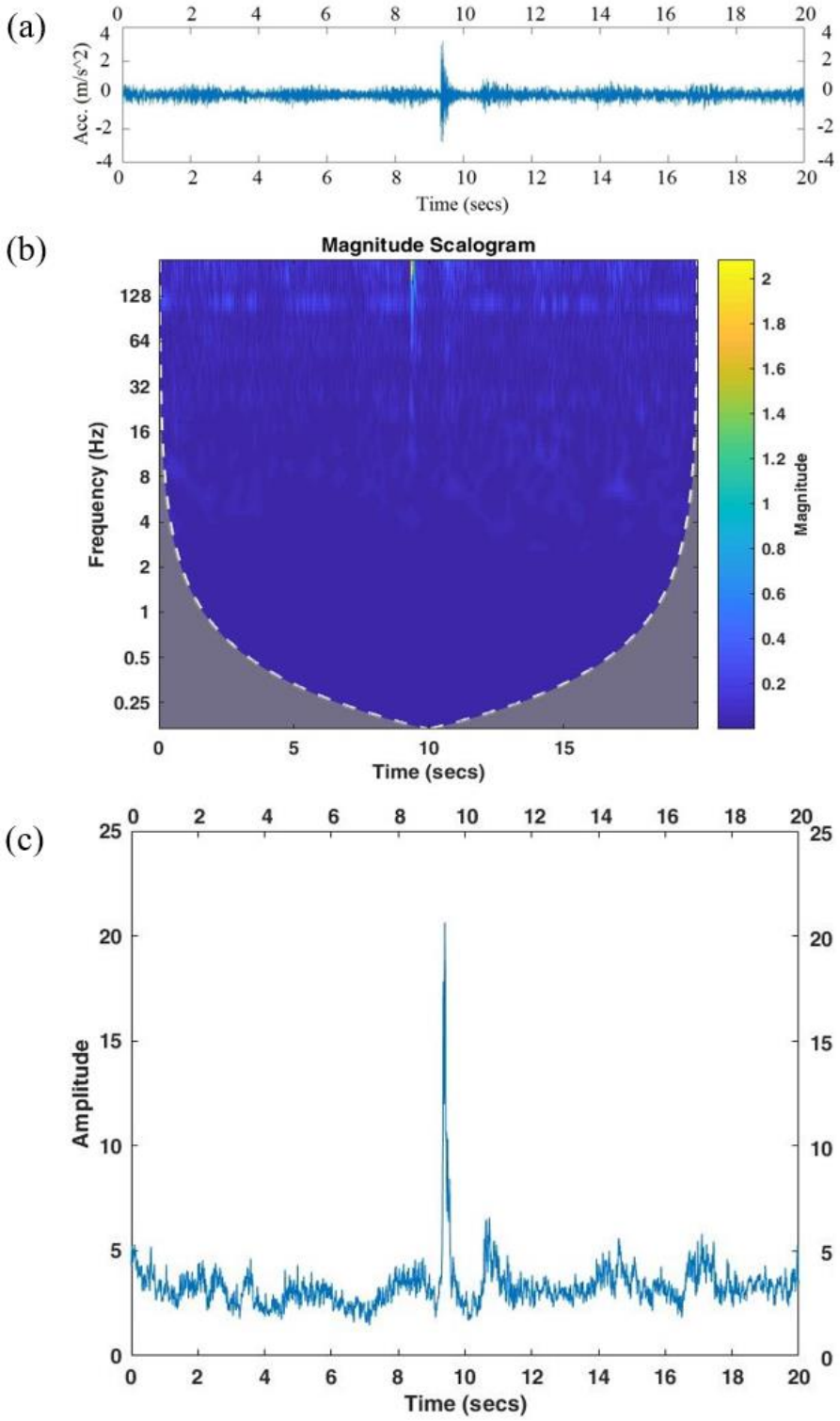

Figure 4.6. Combination of three graphs showing a) Time-series plot, b) Wavelet plot and c) Integration of wavelet respect to frequency, respectively, for NAWRTC GE turbine during normal operation.

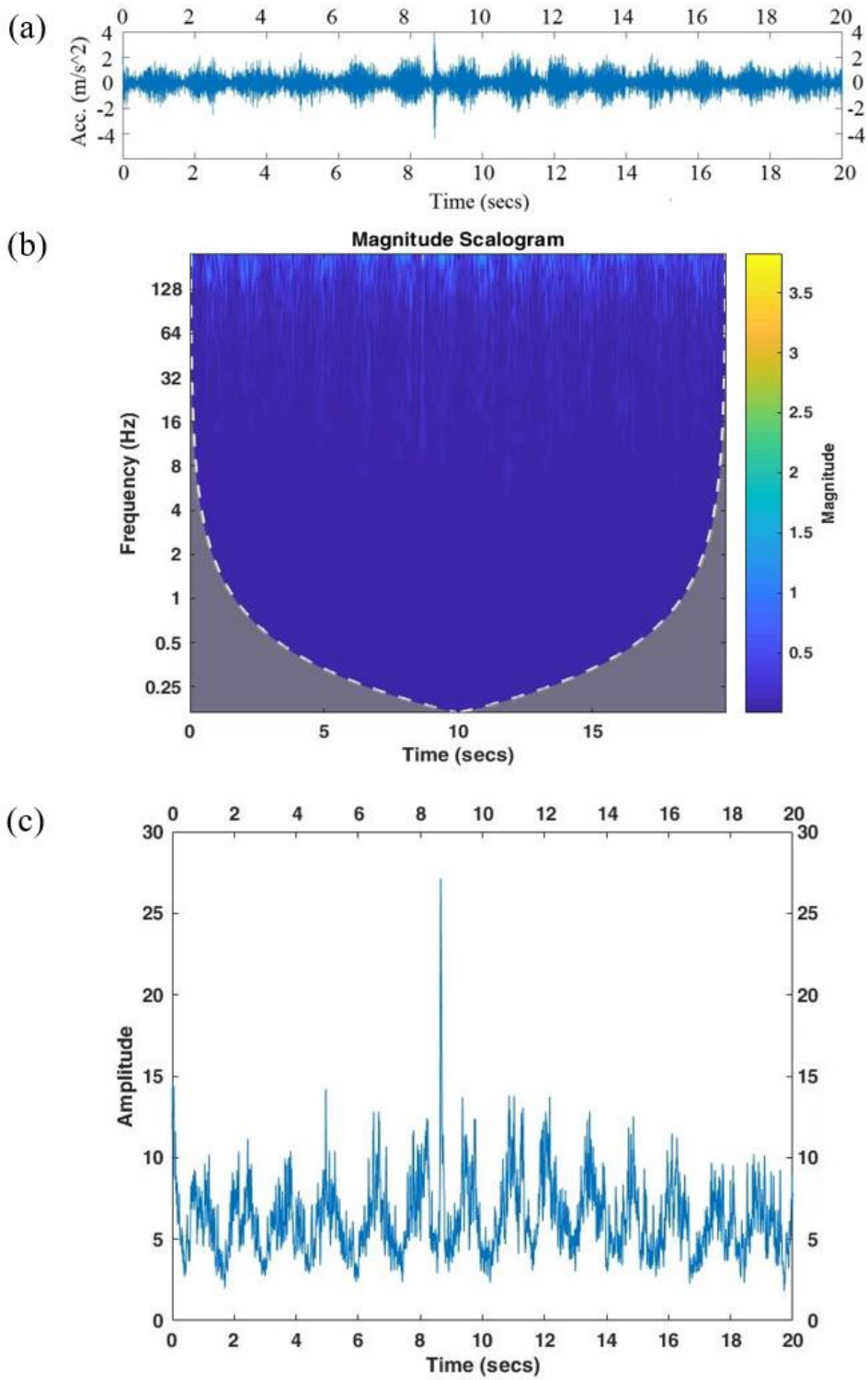

Figure 4.7. Combination of three graphs showing a) Time-series plot, b) Wavelet plot and c) Integration of wavelet respect to frequency, respectively, for NREL CART3 during normal operation.

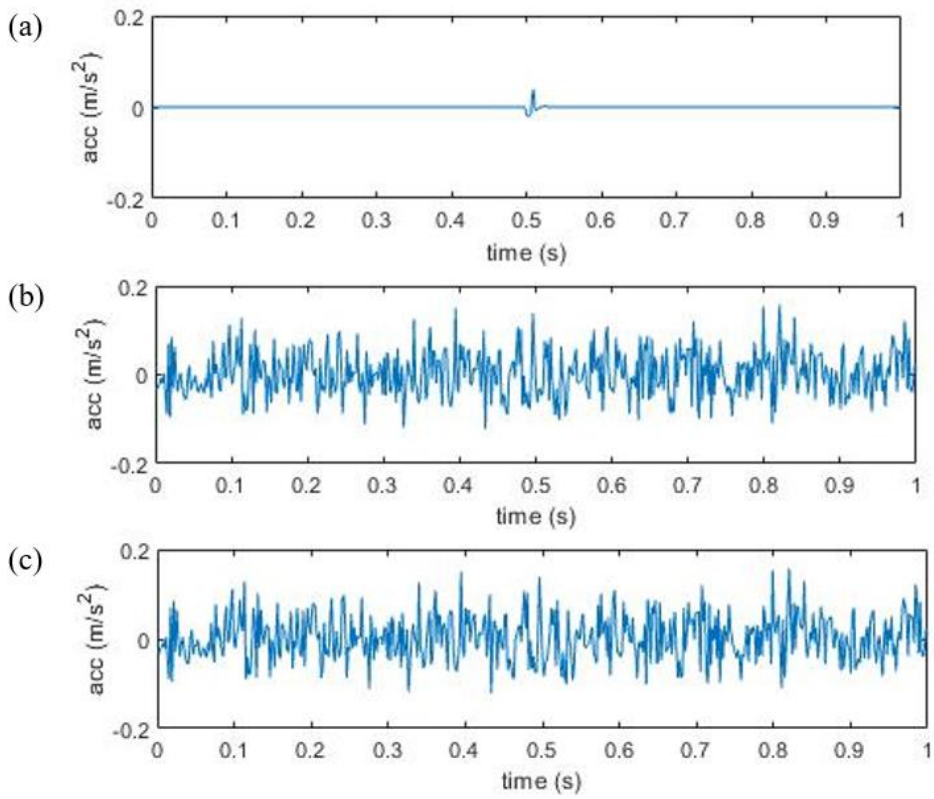

Figure 4.8. The waveform of constructed signal with $SNR = 1.5$: (a) single impact with $\xi = 0.007$ and $f = 512\ Hz$; (b) Gaussian white background noise with zero-mean and 0.05 standard deviation; (c) mixed signal.

4.5 Simulated Studies

Since bird/bat impacts are rare, artificial impacts were created by launching tennis balls using a compressed-air cannon. Ideally, the vibration sensors need to be installed on turbine blades for a sufficient time to obtain both signals with and without artificial impacts. However, even with artificial impacts, only a handful of events were successfully created, as stated in the previous section. The predictive model developed by such imbalanced dataset can be biased and inaccurate [25], especially when the detection of the impact is crucial. Hence, mathematically simulated impact events were

conducted for sufficient number of training examples from both positive (i.e., impact events) and negative (i.e., non-impact events) categories. In the simulation, a single impact signal is defined as

$$s(t) = \begin{cases} 0 & t < 0 \\ \exp\left(-\frac{\xi}{\sqrt{1-2\xi^2}} \cdot 2\pi f t\right) \cdot \sin(2\pi f t) & t \geq 0 \end{cases} \tag{8}$$

where ξ is the damping coefficient, $\frac{\xi}{\sqrt{1-2\xi^2}}$ is the damping attenuation characteristics of impact response, and f is the sampling frequency [32]. The background noise is simulated using Gaussian white noise, which can be characterized by its mean and standard deviation. Figure 4.8 shows the waveform of the simulation signal with $\xi = 0.007$ and $f = 512\ Hz$ for the single impact signal, Gaussian white background noise with zero-mean and 0.05 standard deviation, and the mixed signal, respectively. A total number of 10,000 independent examples (5,000 with impact and 5,000 without impact) were simulated for each level of SNR. The SVM model was built using 10-fold cross-validation and evaluated by traditional evaluation methods including:

$$Accuracy = \frac{TP+TN}{TP+TN+FP+FN} \tag{9}$$

$$Precision = \frac{TP}{TP+FP} \tag{10}$$

$$Recall = \frac{TP}{TP+FN} \tag{11}$$

where TP, TN, FP, FN are true positive, true negative, false positive, and false negative events, respectively. Figure 4.9 and Figure 4.10 show the relationships between SNR and $accuracy$, SNR and $precision$, respectively. In both plots, the first three datapoints ($SNR < 2$) are considered as outliers since an approximate of 50% or less detection rate in a binary classification case indicates nothing more than a random guess. In other words, the predictive model is underfitting when the impact signal is too small. For $SNR \geq 2$, both plots exhibit linear regression relationships between SNR and $accuracy$, SNR and $precision$, respectively. As expected, the overall performance of the predictive model increases as the SNR increases.

It should be noted that in the case of avian species interacting with wind turbines, the detection of impact is crucial for the purpose of bird protection since data and images for event confirmation and species recognition will only be available when the system is triggered [24]. That means the detection system will prefer to detect all actual impacts (i.e., TP plus FN) but can allow some tolerance in the accuracy of non-impact event detection. Hence, $recall$ is of greater importance when evaluating the model performance. Figure 4.11 shows the relationship between SNR and $recall$. The first three datapoints are still considered as outliers despite a detection rate slightly over 50%. For $SNR \geq 2$, the plot also exhibits linear regression relationships between SNR

and $recall$, which is in consistence with the results of performance evaluated by $accuracy$ and $precision$.

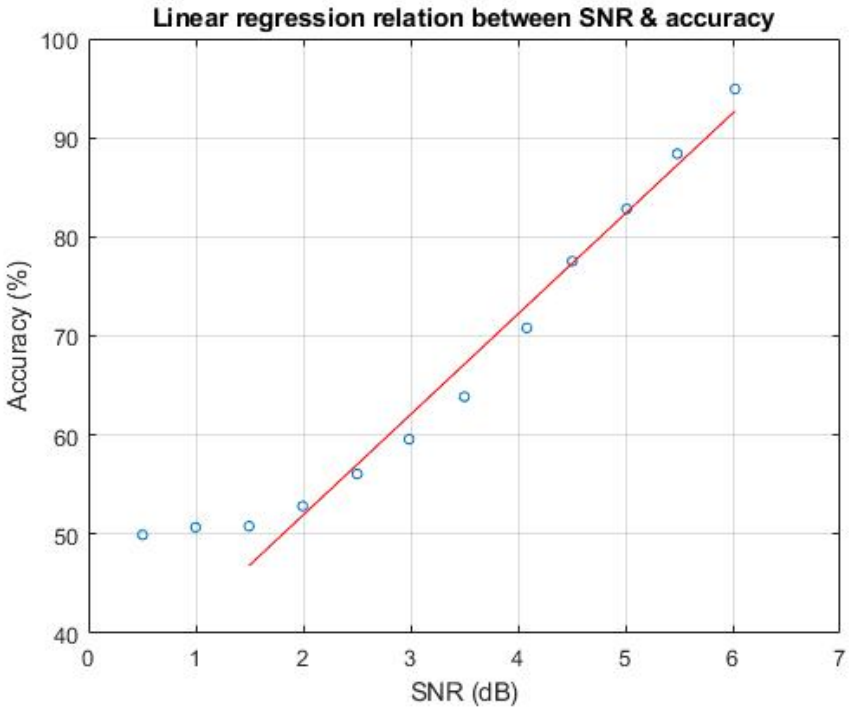

Figure 4.9. Relationship between SNR and accuracy. Each point represents the resultant of 10,000 independent examples.

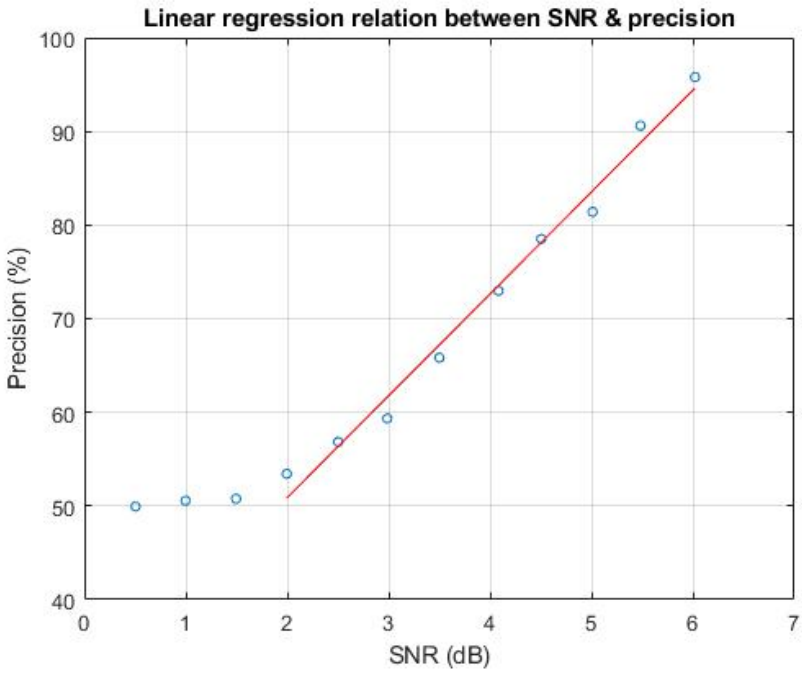

Figure 4.10. Relationship between SNR and precision. Each point represents the resultant of 10,000 independent examples.

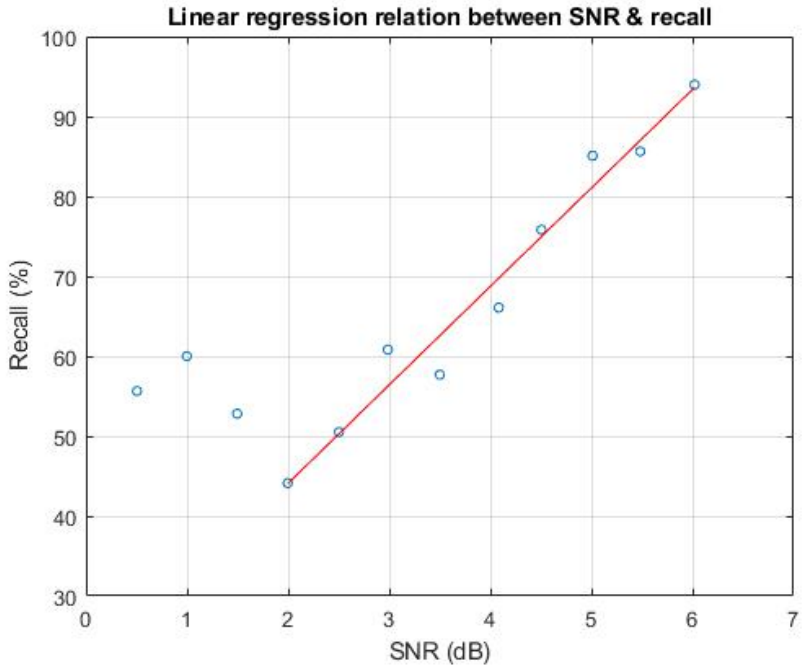

Figure 4.11. Relationship between SNR and recall. Each point represents the resultant of 10,000 independent examples.

4.6 Conclusions

This study demonstrates through both experimentation and simulation the feasibility of impact detection using a conventional SVM model applied to vibration data collected by vibration sensors on wind turbine blades. Field tests were performed on full-scale wind turbines in real operating conditions with simulated bird impact on blades. 14 out of 29 registered artificial impacts were identified on-site by visual inspection and signal processing using the short-time Fourier transform on raw vibration signal time histories, which corresponds to a 48.3% success rate. It elucidates that SNR, together with a fast post-processing technique to discern the spike caused by the impact from the normal vibration background, are critical for real-time automatic impact detection on wind turbine blades. It is necessary to perform simulated studies due to the fact that bird impacts are rare. Simulated studies also allow the performance evaluation of SVM model on lower SNRs, which is not feasible using field testing data since the impact signals are usually indistinguishable. It can be concluded from simulated studies that the proposed SVM model trained by the 18 features extracted from raw vibration time histories and TMI graph can reliably predict whether a sample signal contains an impact or not, with an overall $accuracy$, $precision$ and $recall$ higher than 95% when $SNR \geq 6$. However, the model is not effective when $SNR < 2$.

4.7 Acknowledgements

The authors wish to acknowledge the financial support of the U.S. Department of Energy under DE-EE0005363. The authors are grateful to the staff of the North

American Wind Research and Training Center at Mesalands Community College for contributing to the success of the system's first field test. The authors would also like to express gratitude to the staff and scientists at NREL for their willingness to share information with the team and for use of the Controls Advanced Research Turbines (CART) at the National Wind Technology Center for system testing and demonstration. Finally, we greatly appreciate the review and expert contributions of our science and industry advisory panel.

4.8 References

5 Kumar Y, Ringenberg J, Depuru SS, Devabhaktuni VK, Lee JW, Nikolaidis E, Andersen B and Afjeh A (2016) Wind energy: Trends and enabling technologies. *Renewable and Sustainable Energy Reviews* 53: 209–224.

6 Thaxter CB, Buchanan GM, Carr J, Butchart SHM, Newbold T, Green RE, Tobias JA, Foden WB, O'Brien S andPearce-Higgins JW (2017) Bird and bat species' global vulnerability to collision mortality at wind farms revealed through a trait-based assessment. *Proc. R. Soc. B* 284(1862).

7 Schwartz M, Heimiller D, Haymes S and Musial W (2010) Assessment of offshore wind energy resources for the united states. Technical report, National Renewable Energy Laboratory, Golden, CO.

8 Bailey H, Brookes KL and Thompson PM (2014) Assessing environmental impacts of offshore wind farms: lessons learned and recommendations for the future. *Aquatic Biosystems* 10(1): 8.

9 Thomsen K (2014) *Offshore wind: A comprehensive guide to successful offshore*

wind farm installation. San Diego,CA: Elsevier Science.

10 Korner-Nievergelt F, Brinkmann R, Niermann I and Behr O (2013) Estimating bat and bird mortality occurring at wind energy turbines from covariates and carcass searches using mixture models. *PLOS ONE* 8(7).

11 Parise J and Walker TR (2017) Industrial wind turbine post-construction bird and bat monitoring: A policy framework for canada. *Journal of Environmental Management* 201: 252–259.

12 Zohbi GA, Hendrick P and Bouillard P (2015) Evaluation of the impact of wind farms on birds: The case study of lebanon. *Renewable Energy* 80: 682–689.

13 Smallwood KS (2017) Long search intervals underestimate bird and bat fatalities caused by wind turbines. *Wildlife Society Bulletin* 41(2): 224–230.

14 Grodsky SM, Behr MJ, Gendler A, Drake D, Dieterle BD, Rudd RJ and Walrath NL (2011) Investigating the causes of death for wind turbine-associated bat fatalities. *Journal of Mammalogy* 92(5): 917–925.

15 Loss SR, Will T and Marra PP (2013) Estimates of bird collision mortality at wind facilities in the contiguous united states. *Biological Conservation* 168: 201–209.

16 Kunz T, Arnett EB, Cooper BM, Erickson WP, Larkin RP, Mabee T, Morrison ML, Strickland MD and Szewczak JM (2007) Assessing impacts of wind-energy development on nocturnally active birds and bats: A guidance document. *Journal of Wildlife Management* 71(8): 2449–2486.

17 KSovacool B (2009) Contextualizing avian mortality: A preliminary appraisal of bird and bat fatalities from wind, fossil-fuel, and nuclear electricity. *Energy Policy* 37(6): 2241–2248.

18 Marques AT, Batalha H, Rodrigues S, Costa H, Pereira MJR, Fonseca C, Mascarenhas M and Bernardino J (2014) Understanding bird collisions at wind farms: An updated review on the causes and possible mitigation strategies. *Biological Conservation* 179: 40–52.

19 Sovacool BK, Lindboe HH and Odgaard O (2008) Is the danish wind energy model replicable for other countries? *The Electricity Journal* 21(2): 27–38.

20 Plonczkier P and Simms IC (2012) Radar monitoring of migrating pinkfooted geese: behavioural responses to offshore wind farm development. *Journal of Applied Ecology* 49(5): 1187–1194.

21 Brabant R, Vanermen N, Stienen EWM and Degraer S (2015) Towards a cumulative collision risk assessment of local and migrating birds in north sea offshore wind farms. *Biological Conservation* 756(1): 63–74.

22 Fijn RC, Krijgsveld KL, Poot MJM and Dirksen S (2015) Bird movements at rotor heights measured continuously with vertical radar at a dutch offshore wind farm. *IBIS* 157(3): 558–566.

23 Towsey M, Wimmer J, Williamson I and Roe P (2014) The use of acoustic indices to determine avian species richness in audio-recordings of the environment. *Ecological Informatics* 21: 110–119.

24 Masden EA and Cook ASCP (2016) Avian collision risk models for wind energy impact assessments. *Environmental Impact Assessment Review* 56: 43–49.

25 Marquez FPG, Tobias AM, Perez JMP and Papaelias M (2012) Condition monitoring of wind turbines: Techniques and methods. *Renewable Energy* 46: 169–178.

26 Bassett K, Carriveau R and Ting DS (2011) Vibration response of a 2.3 mw wind turbine to yaw motion and shutdown events. *Wind Energy* 14(8): 939–952.

27 Abouhnik A and Albarbar A (2012) Wind turbine blades condition assessment based on vibration measurements and the level of an empirically decomposed feature. *Energy Conversion and Management* 64: 606–613.

28 Hu C, Albertani R and Suryan RM (2018) Wind turbine sensor array for monitoring avian and bat collisions. *Wind Energy* 21: 255–263.

29 Cristianini N (2000) *An introduction to support vector machines: and other kernel-based learning methods.* Cambridge, New York: Cambridge University Press.

30 Boser BE, Guyon IM and Vapnik VN (1992) A training algorithm for optimal margin classifiers. In: Haussler D (ed.) *Proceedings of the 5th Annual Workshop on Computational Learning Theory (COLT'92)*. Pittsburgh, PA, USA: ACM Press, pp. 144–152.

31 Kumar A and Kumar R (2017) Time-frequency analysis and support vector machine in automatic detection of defectfrom vibration signal of centrifugal pump. *Measurement* 108: 119–133.

32 Shohag MA, Hammel EC, Olawale DO and Okoli OI (2017) Damage mitigation techniques in wind turbine blades: A review. *Wind Engineering* 41(3): 185–210.

33 Sellami T, Berriri H, Darcherif AM, Jelassi S and Mimouni MF (2016) Modal and harmonic analysis of three-dimensional wind turbine models. *Wind Engineering* 40(6): 518–527.

34 Ouanas A, Medoued A, Mordjaoui M, Lebaroud A and Sayad D (2018) Fault diagnosis in yaw drive induction motorfor wind turbine. *Wind Engineering* 42(6):

576–595.

35 Purarjomandlangrudi A, Nourbakhsh G, Esmalifalak M and Tan A (2013) Fault detection in wind turbine: Asystematic literature review. *Wind Engineering* 37(5): 535–546.

36 Liu R, Yang B, Zhang X, Wang S and Chen X (2016) Time-frequency atoms-driven support vector machine method for bearings incipient fault diagnosis. *Mechanical System and Signal Processing* 75: 345–370.

5 MANUSCRIPT 3

Wind turbine event detection by support vector machine

Congcong Hu[1]; Roberto Albertani[1].

Submitted to

Wind Energy

[1]School of Mechanical, Industrial and Manufacturing Engineering, Oregon State University, Corvallis, Oregon, USA

5.1 ABSTRACT

Considering the increase in the deployment of wind energy conversion systems, improving the co-existence between wind turbines and wildlife with an efficient method for blade impact assessment are of primary importance. A heterogeneous multi-sensor system for automatic eagle detection and deterrent, including an automatic blade-event detection module, was developed providing the necessary field data. An automated blade event detection system, based on support vector machine, a form of machine learning, was developed and tested. Training of the algorithm was performed using features extracted from vibration signals and energy distribution graphs obtained from numerical simulations of blade impacts. Performance of the method, evaluated using numerical simulations at different levels of signal-to-noise ratios, relative to artificial impacts, showed the best results when trained using combined raw vibration signal and time marginal integration graphs, exhibiting an overall $accuracy$ of 93% at $SNR = 6$. The proposed model was tailored for improving specificity (i.e. false negative error), a critical aspect for endangered species events. Performance of the trained algorithm evaluating field data exhibited an improvement in impact detection from a visually identifiable rate of 42% to true positive prediction rate of 75%. The system could perform, with appropriate training, diverse functions as components health monitoring or lighting strike automatic monitoring.

5.2 Introduction

One of the major ecological objectives associated with the deployment of wind farms is the improvement of the coexistence of birds and bats with wind turbines [1-5]. While blade collisions rates have been investigated and reported [6, 7], traditional mortality estimates still rely on methods such as long-term visual observation and carcass survey [8-11]. Those methods however are characterized by inherent uncertainties caused mainly by scavengers, low deployment of human observers and the nature of the environment like presence of thick grass, shrubs or on water. Under the aforementioned conditions the estimated mortality rates could contain significant differences from reality [10].

One approach for effective and low-cost automatic detection of bird/bat collision with wind turbines is to apply continuous vibration and noise monitoring on blades by the implementation of vibrational or acoustic sensing devices. The conceptual design of a multi-sensor system that provides both temporal and spatial coverage capacities for auto-detection of bird collision events was carried out at Oregon State University (OSU) based on prior research on bird collision monitoring systems [12, 13]. Vibrations and structural-borne noise data was acquired during field testing on utility-scale wind turbines. Artificial collision events were created by launching tennis balls into moving blades using compressed-air cannon. Preliminary results showed that it is feasible to detect an impact using common vibration sensors by visual inspection. Relatively simple automatic algorithms were applied in the case of high signal-to-noise ratios (SNR) [12]. However, vibration signals that contain low-intensity impacts embedded

in relatively high background noise are characterized by low SNRs, exhibiting low rate or no success in detection. In such cases, more advanced signal processing algorithms need to be developed and tested using experimental data.

Vibration-based monitoring techniques are well developed and widely adopted on modern wind turbines for the main purpose of structural health monitoring [14, 15]. Vibration sensors such as piezoelectric diaphragms and accelerometers are commonly applied for the analysis of dynamic structural response during turbine operations [16]. A significant effort has been devoted by researchers for the detection of faults in rotating parts such as blades, bearings and gearbox under dynamic loads, by identifying its characteristic features in the vibration signal. In such case, signals caused by the defects will have a periodic characteristic. However, when in the occurrence of an abnormal one-time event, typically a blade strike or a lighting strike, the resulting effect is a non-periodic signal. Currently, there are no practical existing methods/techniques for automatic non-periodic event detection.

This paper presents a robust method for automatic detection of non-periodic event under the general framework of structural health monitoring (SHM). Instead of traditional statistical analysis involved in SHM, a predictive model is constructed by implementation of support vector machine (SVM), one of the most widely applied machine learning methods for general classification problems such as condition monitoring and fault diagnosis [17]. The proposed method extracts features from

vibrations signals acquired on wind turbine blades and associated energy distribution graphs. Training of SVM is achieved by running the algorithm on a significant number of impact simulations. Preliminary results obtained by testing the predictive model trained by SVM using simulations of blade impact [18] showed an increasing performance as the SNR increases, as expected. This paper explains further developments in the SVM algorithm training methodologies by conducting simulated studies. Finally, a SVM predictive model was constructed and its performance was evaluated using field data on a commercial 1.5 MW wind turbine with and without impacts on the blades.

5.3 Methods

5.3.1 Support vector machine

Support vector machine is a supervised machine learning method introduced by Vapnik et al. [17, 19]. It is widely applied to specific fault diagnosis of different types of machinery [20]. The method, well known for classification of periodic-type events, was originally defined and applied to non-periodic events such as blade impacts with foreign objects. Using time histories of vibrations and structure-born noise on wind turbine blades, a binary classification problem including two classes of labeled events for training is defined. SVM then is employed to construct a predictive model for new non-labeled events [18].

Given a sample dataset $(x_i, y_i)_{i=1}^{N}$, x_i denotes thei^{th} vector in the input space X and y_i is the label associated with x_i. A hyperplne, in the form of

$$f(x) = w^T x + b = 0, \tag{1}$$

where w is the weight vector and b is the bias, is established to divide the input space X into two classes: positive ($f(x) > 0$) and negative ($f(x) < 0$). Maximum margin criterion is applied to find the optimized hyperplane, which gives the maximum distance between the nearest data and plane, as illustrated in Figure 5.1.

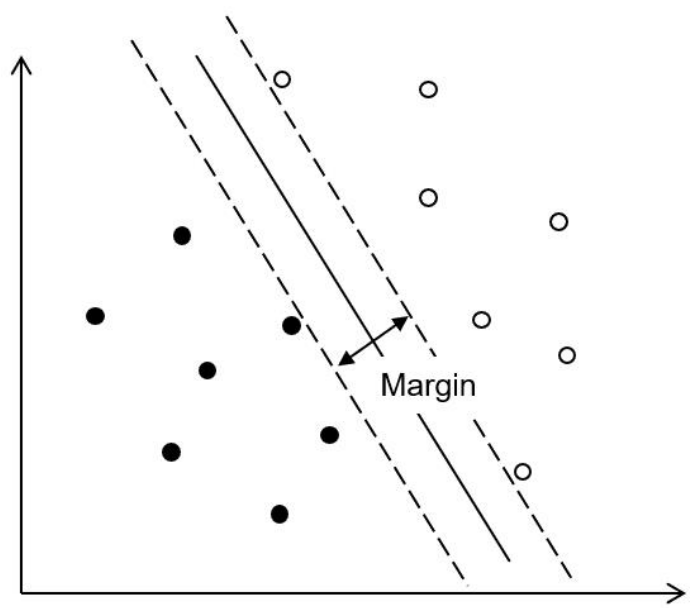

Figure 5.1. Illustration of linear classifier in two-dimensional feature space given by maximum margin criterion.

A Constrained optimization technique also known as soft-margin SVM , coupled with Lagrange dual formulation method are then applied. For data that are non-linearly separable in the input space X, the input vector x_i can be mapped into a higher feature space F by mapping function $\Phi(x)$, making them linearly separable. Since explicitly mapping input vectors from the lower dimensional space into the higher dimensional space can result in quadratic complexity, kernel function $K(x_i, x_j) = \Phi^T(x_i) \cdot \Phi(x_j)$ is introduced to solve the issue by skipping the step of explicitly mapping [17]. Finally, a "kernelized" dual quadratic optimization problem is solved by the sequential minimal optimization [17] method, obtaining the final discriminant function with expression of

$$f(x) = sign(\sum_{i=1}^{N} \alpha_i y_i K(x, x_i) + b). \tag{2}$$

5.3.2 Application to impact detection

The application of the methods described above for automatic impact detection on wind turbine blades starts with the collection of raw time-histories collected by the sensors installed on the wind turbine blades and then processed by continuous wavelet transform (CWT), followed with integrating CWT with respect to time, producing the energy distribution graph, which is also defined as the time marginal integration (TMI) graph [18]. The flow chart of the proposed method is shown in Figure 5.2. A total number of 18 selected statistical features, as listed in Table 5.1, are extracted from the raw signals and TMI graphs, respectively. The predictive model is trained by 10-fold

cross-validation with parameters γ and C optimized by grid search in a grid of $2^{-10} - 2^{10}$.

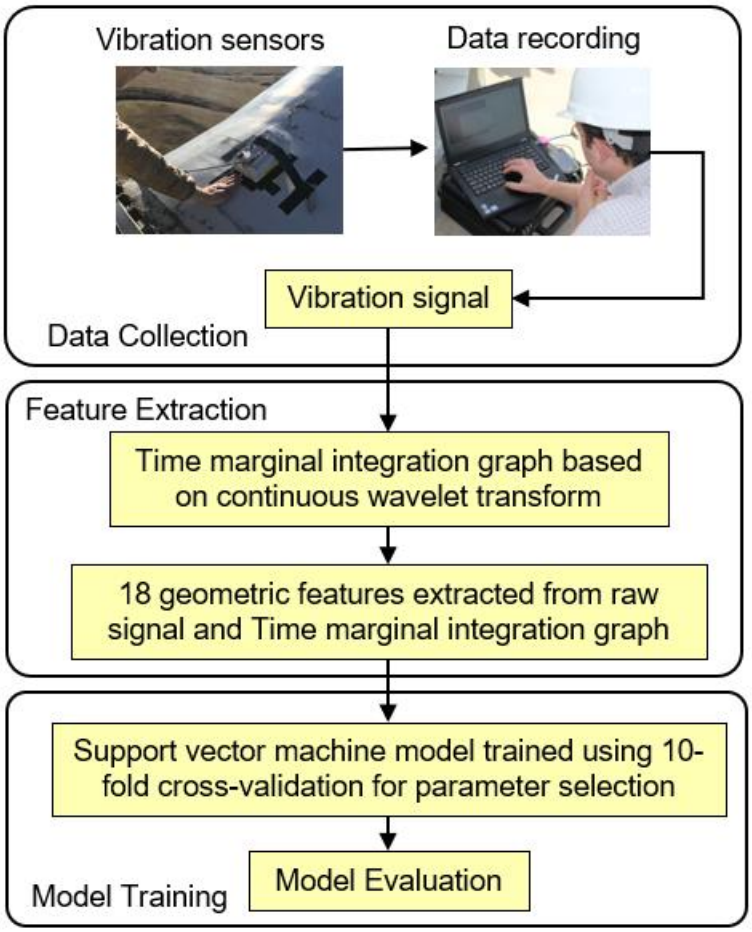

Figure 5.2. Flow chart of proposed method for automatic impact detection on wind turbine blade.

Table 5.1. List of extracted features.

No.	Feature from raw signal	No.	Feature from TMI graph
1	Kurtosis	10	Kurtosis
2	Skewness	11	Skewness
3	Mean	12	Mean
4	RMS	13	RMS
5	Variance	14	Variance
6	Peak	15	Peak
7	Impulse factor	16	Impulse factor
8	Shape factor	17	Shape factor
9	Crest factor	18	Crest factor

5.4 Simulated studies

To verify the validity of the SVM predictive model applied to impact detection, simulation experiments were conducted before its application to field experimental data. Simulations of independent events with and without impact components were performed. Demonstration of the advantage of TMI-based features was carried out. The performance of the model was further evaluated by the receiver operating characteristics (ROC) curve.

5.4.1 Impact simulation

In the simulation, each independent training example is constructed by combining a single impact signal and the background noise. The single impact signal is defined as:

$$s(t) = \begin{cases} 0 & t < 0 \\ \exp\left(-\frac{\xi}{\sqrt{1-2\xi^2}} \cdot 2\pi f t\right) \cdot \sin(2\pi f t) & t \geq 0 \end{cases} \tag{3}$$

where ξ is the damping coefficient, $\frac{\xi}{\sqrt{1-2\xi^2}}$ is the damping attenuation characteristics of impact response, and f is the sampling frequency [21]. The background noise is simulated using Gaussian white noise characterized by its mean and root mean square (RMS) value. Signals are characterized by different SNR levels, which depend on impact signal intensities and background vibrations. The SNR is defined as follows:

$$SNR = 20log_{10}\frac{A_{impact}}{A_{noise}} \tag{4}$$

where$A$ denotes the RMS amplitude. Figure 5.3 illustrates simulated training example signals of the pure impact with $\xi = 0.007$ and $f = 512\,Hz$, Gaussian white background noise with zero-mean and 0.05 RMS, and the resulting combined

waveform, respectively. The impact of SNR = 1.5, which occurred at time = 0.5 s, was embedded in a noisy signal. For each level of SNRs (12 different levels from SNR = 0.5 to SNR = 6 with an increment of 0.5), a total number of 10,000 independent examples (5,000 with impact and 5,000 without impact) were simulated.

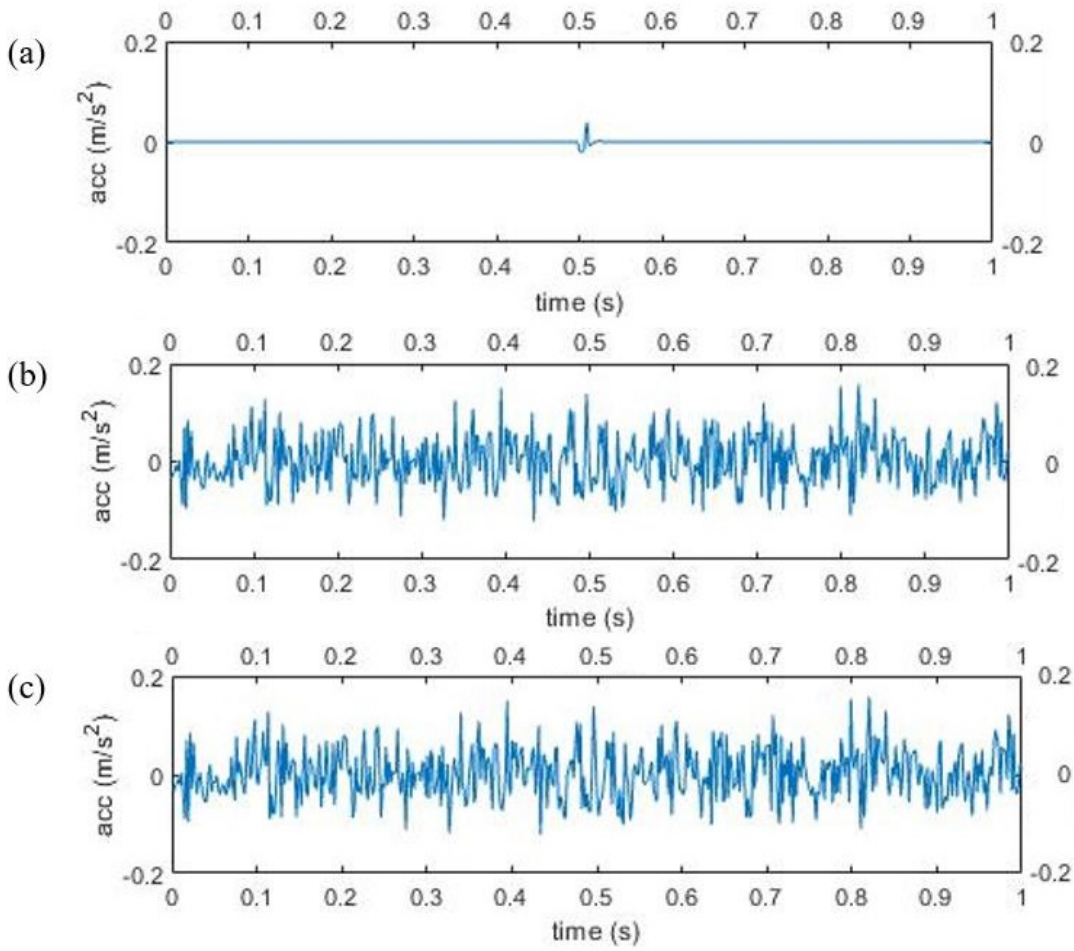

Figure 5.3. Result of an example of the construction of a simulated blade impact with the waveform of combined signal with SNR=1.5: (a) Single impact with $\xi = 0.007$ and $f = 512\ Hz$, (b) Gaussian white background noise with zero-mean and 0.05 root mean square, and (c) Resulting mixed signal.

5.4.2 Performance evaluation

The SVM model was trained with 10-fold cross-validation, and evaluated by overall accuracy [18] and receiver operating characteristics (ROC) curve. Figure 5.4 shows the relationships between SNR and accuracy. As expected, the overall accuracy of trained SVM model increases as the SNR increases, exhibiting linear regression relationships. Furthermore, to demonstrate the advantage of TMI-based features, the accuracy of the model trained by combined raw and TMI features was compared with the models trained by raw features only and TMI features only, respectively. The prediction results of SVM for features extracted from different stages are shown in Figure 5.4. At SNR = 6, the accuracy of the model trained by raw features was 80.32%, while the accuracy of the model trained by TMI features was 91.46%. The model trained by combined features showed the best performance of 93.98% in accuracy, but only a modest increase in respect to TMI features only model.

ROC plot is a graphical plot that shows relative trade-off between true positive rate and false positive rate [21]. It is obtained by plotting the sensitivity against 1 - specificity. The sensitivity, also known as the true positive rate, is a measure of the fraction of actual positives which have been classified as such. The specificity, also known as the true negative rate, measures the fraction of actual negatives correctly classified as such. They are mathematically expressed as:

$$Sensitivity = \frac{TP}{TP+FN}, \tag{5}$$

$$Specificity = \frac{TN}{TN+FP}, \tag{6}$$

where TP, TN, FP and FN are true positive, true negative, false positive and false negative events, respectively. The obtained ROC plot for each selected level of SNR is shown in Figure 5.5. It can be noted from Figure 5.5 that as SNR increases, the points move towards the top-left corner, which represents a perfect model with 100% rate in both sensitivity and specificity. For $SNR < 2$, in the three cases of $SNR = 0.5$, 1 and 1.5, the data points are close to the diagonal line (i.e. 50% random guess line), indicating the model is inefficient and under-fitting.

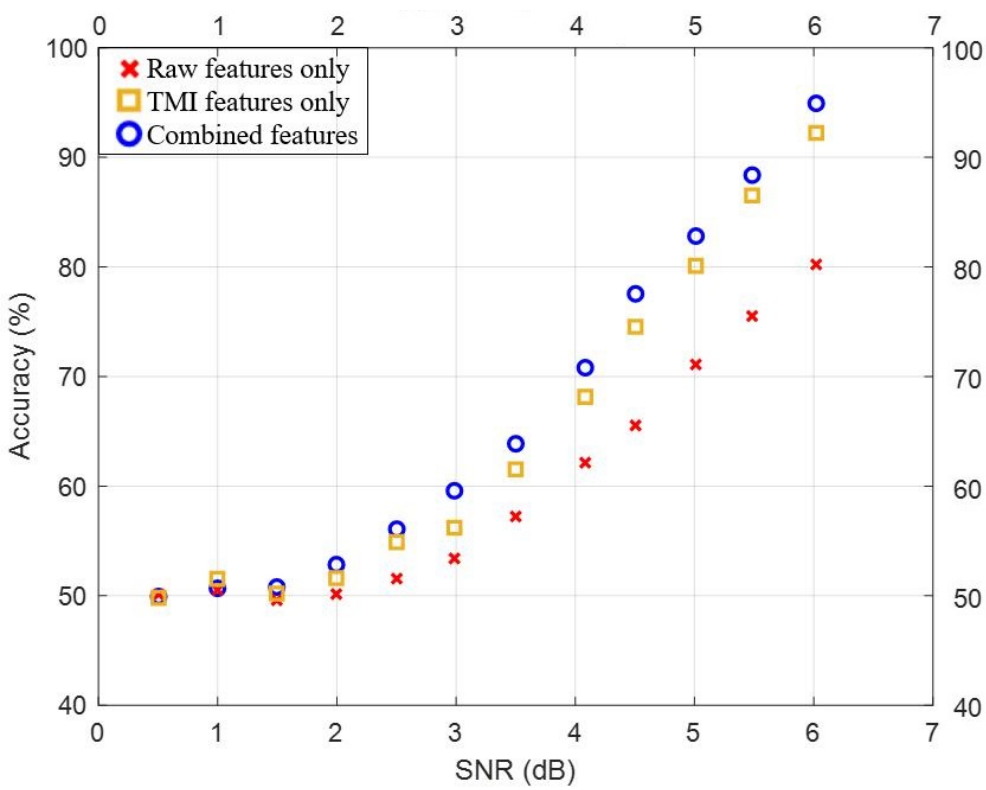

Figure 5.4. Impact simulation results showing relationship between SNR and accuracy for three different cases of model training.

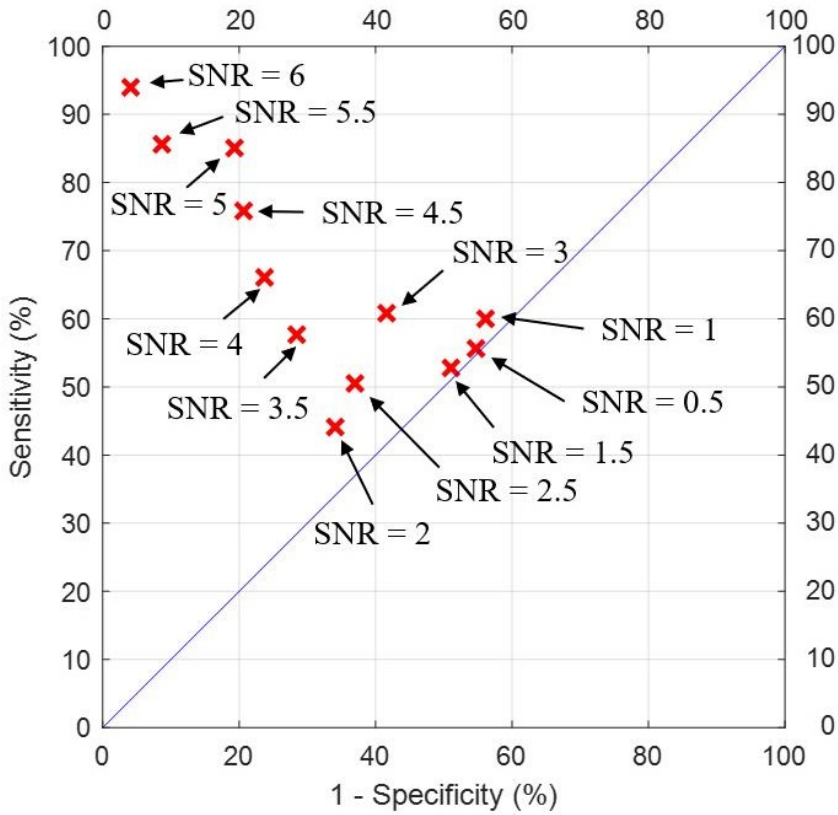

Figure 5.5. ROC graphs showing classification performance of the proposed method using simulation data.

5.5 Experimental evaluation

5.5.1 System overview

A heterogeneous multi-sensor system with specific capabilities of eagle detection and identification, eagle deterrent and blade collision detection has been recently developed [23]. The system mainly consists of three modules as shown in Figure 5.6. The monitoring of the airspace surrounding a wind turbine is performed by the first module, a 360-degree field of view commercial camera. The camera module provides real-time feedback about the presence of moving objects, eagle identification and their flight

paths with respect to the turbine structure. Once a moving object is detected with sufficient number of pixels, eagle identification can be carried out by computer vision deep-learning techniques [23]. In a positive event of eagle flying towards the wind turbine, kinetic inflatable visual deterrents on the ground will be deployed automatically. The third module is a weather-proof blade impact detection (BID) unit installed at the root of each blade as shown in Figure 5.7. The module includes vibration sensors, an accelerometer and a contact microphone, providing continuous structural vibration monitoring used for blade collision detection. The InvenSense MPU-9250 MEMS triple axis accelerometer, forming an inertial measurement unit (IMU) is rigidly attached inside the BID unit with two axes (Y and Z) being in-plane in respect of the blade and parallel to the chord line and X axis off-plane. The contact microphone (CUI Inc. CEB-27D44) is a piezoelectric diaphragm that consists of a piezoelectric ceramic plate. Being attached to the blade surface using adhesive tapes, the deformation of the piezoelectric ceramic plate caused by surface vibrations induces the electric charge. In addition, the BID unit contains a on-blade surveillance camera that provides visual images for potential taxonomic identification.

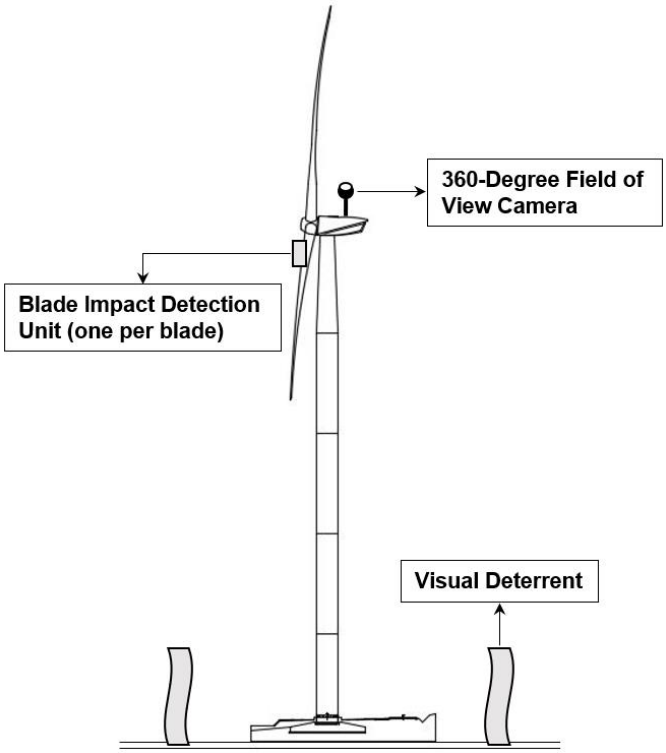

Figure 5.6. Eagle detection, deterrent and blade event detection system diagram.

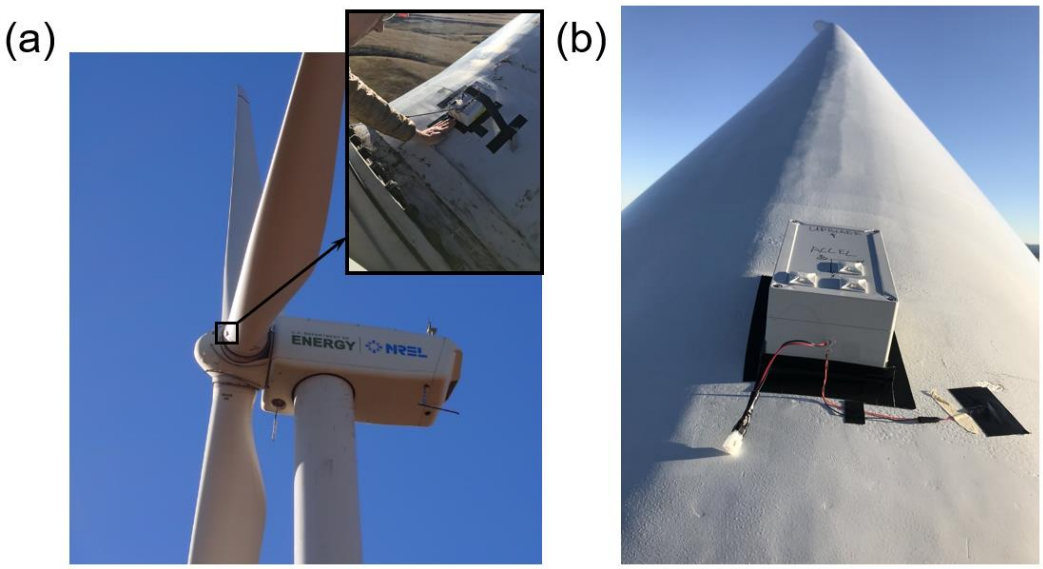

Figure 5.7. Blade impact detection unit installed at the root of each blade on the GE 1.5 MW at the NREL National Wind Technology Center

5.5.2 Field testing summary

The overall system functionality and reliability were validated by field tests at the National Renewable Energy Laboratory (NREL) National Wind Technology Center (NWTC) in Boulder, CO and at the North American Wind Research and Training Center (NAWRTC) at the Mesalands Community College in Tucumcari, NM, both on a General Electric (GE) 1.5 MW wind turbine. Artificial impacts were created by launching tennis balls and small potatoes using a custom compressed-air cannon [12, 13]. Sample plots of raw vibration recordings from the three blades on the GE 1.5 MW at the NWTC are illustrated in Figure 5.8. The top three time histories represent the voltage time histories recorded by the contact microphones, and bottom three represent X axis (i.e. out-of-plane axis) accelerations recorded by the accelerometers. The tests were under low-wind speed conditions and with the rotor in slow wind milling rotation. The figures show the impact occurring on Blade #1 was clearly visible due to the relatively high SNRs, 14.1 and 4.4 for contact microphone and accelerometer respectively. Due to the low background vibration noise and high impact intensity, sensors on Blade #2 and Blade #3 were also able to capture this impact with relatively lower SNRs. The impact cannot be easily discerned from noise and signal spikes from Blade #2 signal from the contact microphone. Cases of data with extremely high noise in the signals or multiple random spikes, were classified as N/A.

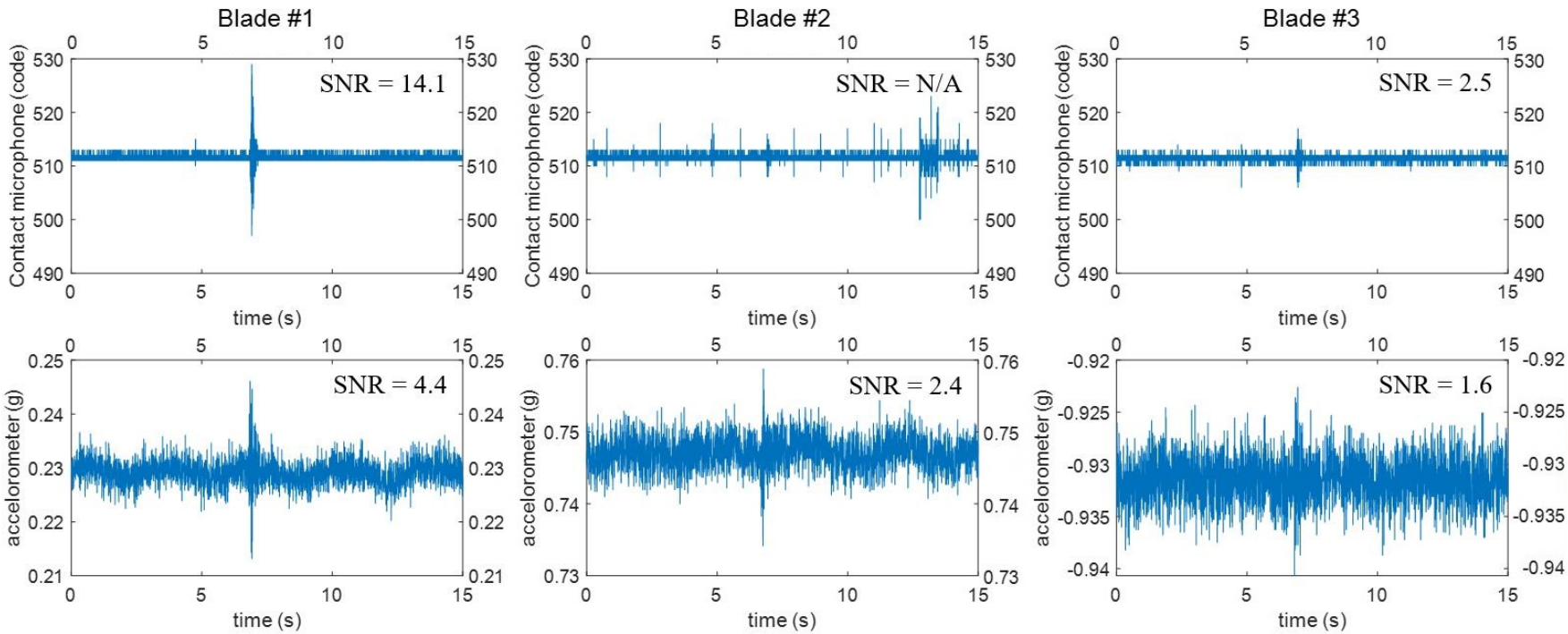

Figure 5.8. Vibration signals from contact microphones (upper plots) and accelerometers (lower plots) with impact occurred on blade #1.

In summary, 13 artificial impacts with tennis balls at NWTC and 13 at NAWRTC were successfully obtained and manually annotated during wind turbines normal operation. Preliminary inspection showed that 11 over the total 26 impact events can be visually identified by any of the recorded raw signals with calculated SNRs in a range between 1.3 and 25.4 with an average of 6.3. Field notes show that most of the identified impacts occurred at the leading edge of the turbine blade thus at a relatively high kinetic energy, while impacts concealed by signal noise and with significantly low SNRs were usually located closer to the rotor shaft at low kinetic energy.

5.5.3 Application

5.5.3.1 Data preparation and model training

Characteristically for a supervised machine learning method, a SVM predictive model requires a substantial number of training examples from all classes to modify and optimize its non-probabilistic linear classifier. In real applications, the vibration sensors would be installed on turbine blades for a sufficient long period of time to obtain vibrations with and without impacts. Since the blade impacts obtained during field tests were not sufficient for an efficient training of the predictive model, a large number of signals with and without impacts were mathematically simulated for training purposes. The simulated signals, characterized by RMS of the background noise and SNR of the impact, were created to replicate the characteristics of the actual signals.

Preliminary inspection on all impact signals indicated a higher reliability of accelerometer signals since contact microphone data exhibited random noise such as multiple spikes shown in Figure 5.8 Blade #2, which can be misclassified as false positive impacts. The three-axis acceleration data showed a wide variation of RMS and SNR due to different test sites, changing weather and turbine operating conditions. To avoid attributes in larger numeric ranges dominating those in lower ranges, the out-of-plane X axis acceleration data from the NAWRTC tests with similar signal properties were selected for valid evaluation of the proposed method. The 13 sets of actual impact signals from NAWRTC, each containing three X-axis acceleration signals from the three respective blades, were selected for the evaluation of the SVM predictive model. A high-pass filter with cutoff frequency of 5 Hz was applied to acceleration signals to eliminate low-frequency components caused by blade rotation, as illustrated in Figure 5.9. All signals were offset to zero to avoid numerical difficulties in calculation. The calculated RMS values range from 0.0020 to 0.0027 with an average SNR of 2.7 for all identifiable impacts.

A total number of 10,000 independent examples (5,000 with impact and 5,000 without impact) were simulated with zero-mean, RMS of 0.0027 g and a fixed SNR of 2.7. The predictive model was trained using those examples by 10-fold cross-validation.

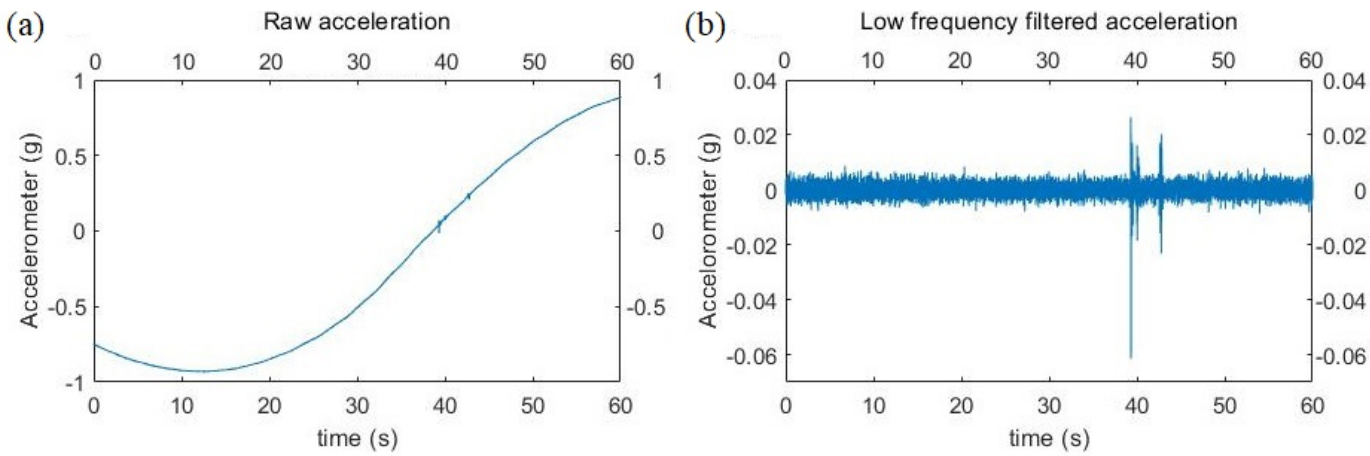

Figure 5.9. Illustration of a high-pass filter. (a) Raw acceleration signal recorded by the accelerometer installed on Blade #2 during an impact. (b) After the application of a high-pass filter with cutoff frequency of 5 hz, low frequency components caused by blade rotation was eliminated.

5.5.3.2 Results

It was determined that testing the predictive model, obtained as explained above, with real vibrations signals was critical, thus the constructed model was evaluated using 13 actual impacts. For testing purpose 1,000 extra independent examples (500 with impact and 500 without impact) were simulated by the same parameters as used in the training dataset simulation, and were added to each actual impact to construct a rich testing dataset. This step provides a larger base of testing examples for the overall accuracy evaluation, which is necessary in determining if a model is reliable or under-fitting. The labels of the 13 actual impacts as predicted by the proposed model including overall accuracy are listed in Table 5.2. Although all actual impacts were predicted as impacts by any of the three-axis acceleration, impact #6, #9 and #10 showed significantly lower overall accuracy (approximately 50%), indicating the model is underfitting, hence their results were considered invalid. The reason for low accuracy

was attributed to high signal noise level. Figure 5.10 shows graphically the overall results of our validation runs. Excluding impact #8, 75% of the actual impacts (nine out of 12) were successfully predicted, including those impacts signal concealed by the background noise, compared to 42% of the actual impacts (five out of 12) identified by visual inspection or detectable by simpler algorithms. Figure 5.11 illustrates a sample of a non-identifiable signal that was successfully predicted to contain an impact with an overall accuracy of 99%.

Table 5.2. Predictive labels of the 13 actual impacts by the predictive model.

Impact #	Blade #1	Blade #2	Blade #3	Overall Accuracy
1	1	N/A	N/A	100%
2	1	1	-1	99%
3	1	-1	-1	97%
4	1	1	-1	99%
5	1	-1	-1	98%
6	1	1	1	Approximately 50%
7	N/A	1	1	99%
8	N/A	N/A	N/A	N/A
9	1	1	1	Approximately 50%
10	1	N/A	N/A	Approximately 50%
11	1	N/A	N/A	99%
12	1	N/A	N/A	99%
13	-1	1	-1	98%

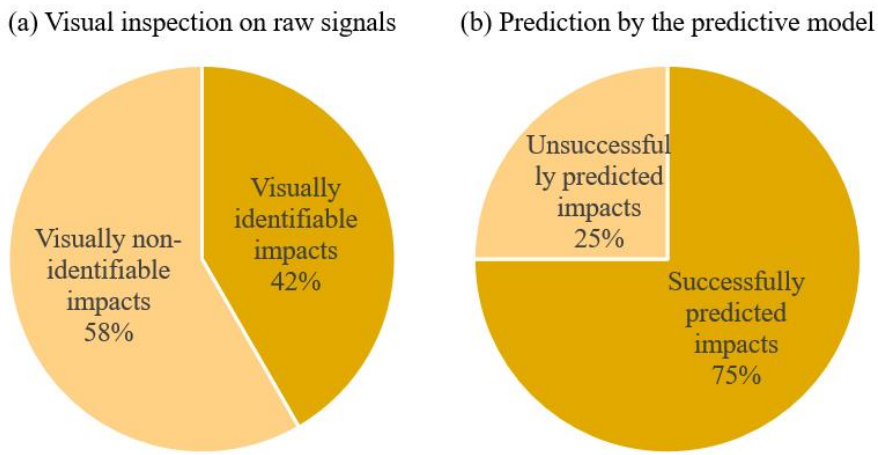

Figure 5.10. Results in percentage of identifiable impacts by: (a) visual inspection; (b) the constructed predictive model.

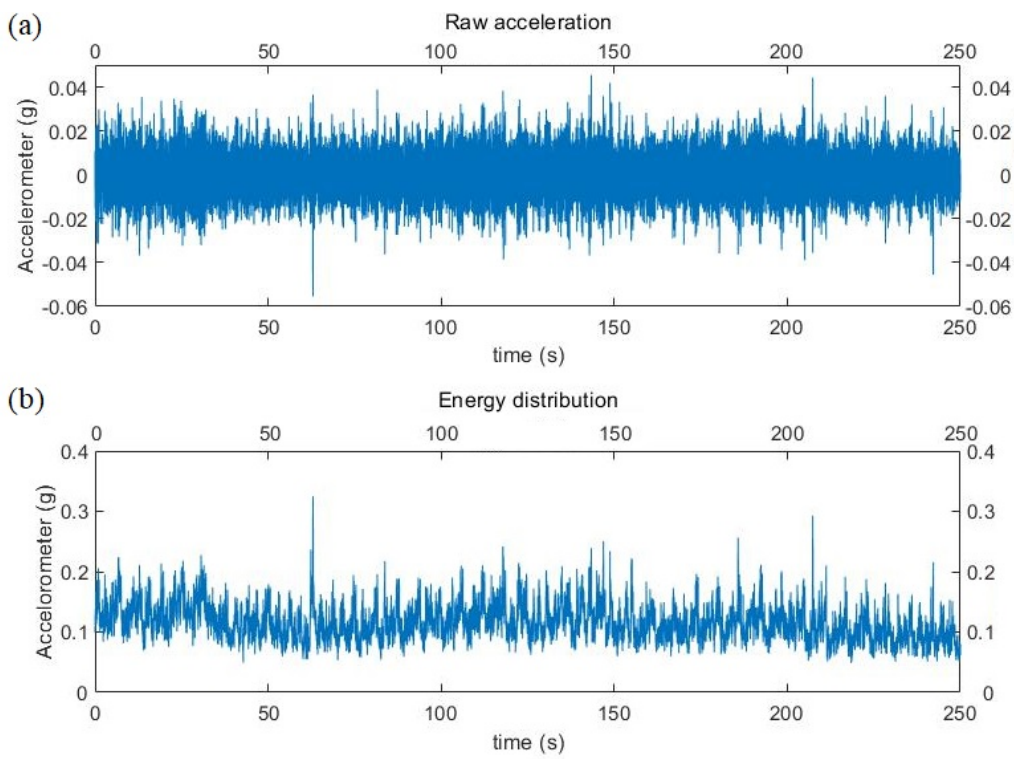

Figure 5.11. Graphs of (a) raw acceleration time-histories and (b) energy distribution of impact #12 on blade #1. The impact was visually non-identifiable but was successfully predicted by the predictive model.

5.6 Conclusions

This study demonstrates the feasibility of the proposed SVM model for detection of blade impact signals concealed in background noise using vibration data collected by conventional sensors (accelerometer and contact microphone) installed on wind turbine blades. Field tests were performed on commercial wind turbines in operating conditions with addition of artificial impacts of tennis balls on blades. Considering the collected data base of confirmed artificial impacts, 11 out of 26, with an average calculated SNR of 6.3, were identified by visual inspection. Those impacts could be alternatively automatically detected by simple automatic algorithms. Simulated operational vibrations with and without impact showed that the proposed SVM model formulated from features extracted from raw and TMI signal has been found to be effective in automatic impact detection in low SNR when the impact is embedded in the background vibration noise, and virtually invisible from inspection. Field impacts augmented by a number of mathematically simulated impacts, at different levels of SNRs, including at extremely low levels of SNRs, showed that the proposed SVM model can effectively detect and classify an abnormal one-time (non-periodic) event as an impact with sufficient accuracy for relatively low levels of SNRs. Considering a $SNR \geq 6$, the overall accuracy can be higher than 93%. Results also showed approximately 50% of accuracy for $SNR < 2$, which indicates the model limit reaching random guess in a binary classification problem. Random guess boundary was also proved by the ROC plot illustrating model results close to the diagonal random guess line for $SNR < 2$. Comparison between predictive models formulated by three different feature sets showed the best results for the model trained using combined

features extracted from both raw vibration signal and TMI graph. TMI-only feature however showed results close to the combination of the two while using raw features only exhibited the lowest performance. Additionally, considering a real case of impact detection between an endangered specie and wind turbine blade, the occurrence of false negative is considered more critical than the occurrence of false positive. In this respect, the specificity is considered more critical than sensitivity. Although $SNR = 5.5$ has approximately the same sensitivity (i.e. false positive error) as $SNR = 5$, the model is superior in improving specificity (i.e. false negative error). Finally, the predictive model trained by simulated signals was evaluated using field data from NAWRTC. Results showed an overall true positive impact detection of 75% compared to 42% of the actual impacts identified by visual inspection or detectable by simpler algorithms, validating that concealed (not visible) impacts can be successfully identified by the proposed predictive model. Alternative training of the same algorithm can perform different tasks as blade structural health monitoring, lighting strike or hail impact automatic monitoring. The system is designed to be turbine-agnostic thus it can be installed and implemented at any time of the turbine operational life or deployment.

5.7 Future work

As concluded, the proposed model with the current training is not effective for extremely low levels of $SNR < 2$. Potential improvements of the system include:

- Algorithm optimization for real time operations;
- Establish new features with stronger correlations with the characteristics of an impact event need in the presence of significant background vibrations noise;

- Increase field data collection to improve model training and possibly identifying new features;
- Installing multiple sensors at different positions per blade and on nacelle and apply sensor fusion techniques to improve impact signal detection. Optimization studies with the objective of establishing the minimum number of vibration sensors on blades for optimum performance and minimum cost could also be beneficial.

5.8 Acknowledgments

The authors would like to acknowledge, and thank, the U.S. Department of Energy Office of Energy Efficiency and Renewable Energy for financial support under contract DE-EE0007885 Wind Energy - Eagle Impact Minimization Technologies and Field Testing Opportunities. The authors are also grateful to the staff at the NREL National Wind Technology Center and at the North American Wind Research and Training Center at Mesalands Community College for their support and guidance during the system's field tests and data acquisition on their wind turbines.

5.9 References

1. Bailey H, Brookes KL, Thompson PM. Assessing environmental impacts of offshore windfarms: lessons learned and recommendations for the future. *Aquatic Biosystems* 2014;10(1): 8.
2. Thomsen K. *Offshore wind: A comprehensive guide to successful offshore wind farm installation*. San Diego, CA: ElsevierScience.2014.
3. Zohbi GA, Hendrick P, Bouillard P. Evaluation of the impact of wind farms on

birds: The case study of Lebanon. *Renewable Energy* 2015; 80: 682–689.

4. Grodsky SM, Behr MJ, Gendler A, et al. Investigating the causes of death for wind turbine-associated bat fatalities. *Journal of Mammalogy* 2011; 92(5): 917–925.
5. Loss SR, Will T, Marra PP. Estimates of bird collision mortality at wind facilities in the contiguous United States. *Biological Conservation* 2013; 168: 201–209.
6. K.Sovacool B. Contextualizing avian mortality: A preliminary appraisal of bird and bat fatalities from wind, fossil-fuel, and nuclear electricity. *Energy Policy* 2009; 37(6): 2241–2248.
7. Marques AT, Batalha H, Rodrigues S, et al. Understanding bird collisions at wind farms: An updated review on the causes and possible mitigation strategies. *Biological Conservation* 2014; 179: 40–52.
8. Korner-Nievergelt F, Brinkmann R, Niermann I, Behr O. Estimating bat and bird mortality occurring at wind energy turbines from covariates and carcass searches using mixture models. *PLOSONE* 2013; 8(7).
9. Parisé J, Walker TR. Industrial wind turbine post-construction bird and bat monitoring: A policy framework for Canada. *Journal of Environmental Management* 2017; 201: 252–259.
10. Smallwood KS. Long search intervals underestimate bird and bat fatalities caused by wind turbines. *Wildlife Society Bulletin* 2017; 41(2): 224–230.
11. Kunz T, Arnett EB, Cooper BM, et al. Assessing Impacts of Wind-Energy Development on Nocturnally Active Birds and Bats: A Guidance Document. *Journal of Wildlife Management* 2007; 71(8): 2449–2486.
12. Hu C, Albertani R, Suryan RM. Wind turbine sensor array for monitoring avian

and bat collisions. *Wind Energy* 2018; 21: 255–263.

13. Flowers J, Albertani R, Harrison T, Polagye B, Suryan RM. Design and Initial Component Tests of an Integrated Avian and Bat Collision Detection System for Offshore Wind Turbines. In: Marine Energy Technology Symposium.; April15–18, 2014; Seattle, WA.
14. Ciang CC, Lee JR, Bang HJ. Structural health monitoring for a wind turbine system: a review of damage detection methods. Measurement Science and Technology 2008; 19(12): 122001.
15. Yang W, Tavner PJ, Crabtree CJ, Feng Y, Qiu Y. Wind turbine condition monitoring: technical and commercial challenges. *Wind Energy* 2014; 17(5): 673-693.
16. Martinez-Luengo M, Kolios A, Wang L. Structural health monitoring of offshore wind turbines: A review through the Statistical Pattern Recognition Paradigm. *Renewable and Sustainable Energy Reviews* 2016; 64: 91-105.
17. Cristianini N. *An introduction to support vector machines: and other kernel-based learning methods*. Cambridge, NewYork: Cambridge University Press. 2000.
18. Hu C, Albertani R. Machine learning applied to wind turbine blades impact detection. *Wind Engineering* 2019.
19. Boser BE, Guyon IM, Vapnik VN. A Training Algorithm for Optimal Margin Classifiers. In: Haussler D., ed. *Proceedings of the 5th Annual Workshop on Computational Learning Theory (COLT'92)* ACM Press; 1992; Pittsburgh, PA, USA:144–152.
20. Widodo A, Yang BS. Support vector machine in machine condition monitoring and

fault diagnosis. *Mechanical Systems and Signal Processing* 2007; 21(6): 2560-2574.

21. Liu R, Yang B, Zhang X, Wang S, Chen X. Time-frequency atoms-driven support vector machine method for bearings incipient fault diagnosis. *Mechanical System and Signal Processing* 2016; 75: 345–370.
22. Yonelinas AP. Receiver-operating characteristics in recognition memory: Evidence for a dual-process model. *Journal of Experimental Psychology* 1994; 20(6): 1341–1354.
23. Albertani R, Johnston M, Todorovic S, Huso M, Katzner T. Eagle Detection, Identification and Deterrent, with Blade Collision Detection for Wind Turbines. In: Wind Wild life Research Meeting XII. AWWI.; Nov.27–30, 2018; St Paul, MN.